

UNIVERSITE KASDI MERBAH OUARGLA

Faculté des Sciences Appliquées
Département de Génie Electrique



Mémoire

MASTER ACADEMIQUE

Domaine : Sciences et technologies

Filière : Génie électrique

Spécialité : Electrotechnique Industrielle

Présenté par :

MAATALLAH Sibaouih

DAHADJ Abdelghani

THEME:

Design and optimization of an off-grid hybrid
PV/wind/Fuel cell power system for remote
areas

Soutenu publiquement

Le : 09/07/2019

Devant le jury :

M^f BOUDJELLA Houari

MAA

Président

UKM Ouargla

M^f DERNOUNI Mhamed

MAA

Encadreur/rapporteur

UKM Ouargla

M^f BENAOUADJ Mahdi

MCB

Examineur

UKM Ouargla

Année universitaire 2018/2019

Table of Contents

List of Figures	iv
List of Tables	vi
Acknowledgment	vii
Nomenclature	viii
Introduction (study motivations)	2
Chapter I: Literature Review	5
I.1 Introduction:	5
I.2 Bibliographic review:	5
I.3 Power sources definitions:	7
I.3.1 Solar power:	7
I.3.2 Wind Energy and Wind Power	12
I.3.3 Storage system	14
I.4 Potential and applications of renewable energy in Algeria	16
I.4.1 Solar Energy:	17
I.4.2 Wind Energy:	18
I.5 Chapter summary:	20
Chapter II: Design and Optimization Method	22
II.1 Introduction:	22
II.2 Load background:	22

II.2.1 Case study:.....	22
II.2.2 Load descriptions:.....	23
II.3 Methods and material.....	25
II.3.1 HOMER energy software:	25
II.4 . Chapter summary:.....	36
CHAPTER III: Power System Modeling	38
III.1 Introduction:.....	38
III.2 System modeling:.....	38
III.2.1 Solar PV Modeling :	38
III.2.2 Wind turbine modeling:	53
III.2.3 PEM fuel cell modeling:.....	57
III.3 Chapter summary:	59
CHAPTER IV: Results and Discussion.....	61
IV.1 Introduction:	61
IV.2 System optimization and simulation.....	61
IV.2.1 Optimum Systems descriptions:	64
IV.2.2 System Architecture	64
IV.2.3 System power sources :	66
IV.2.4 Electrical Summary:	72
IV.2.5 System economical aspect:.....	74
IV.2.6 PV/wind/FC based system VS diesel generator based system:	75
IV.3 Chapter summary.....	77

Bibliography:99

List of Figures

Fig I.1 The enabling environment for scaling up off-grid solutions6

Fig I.2 Monocrystalline Solar Panels (Mono-SI) [6].....8

Fig I.3 Polycrystalline Solar Panels (Poly-SI) [6].....9

Fig I.4 Thin-Film Solar Cells (TFSC) [6].....10

Fig I.5 Concentrated PV Cell (CVP and HCVP) [6]12

Fig I.6 horizontal Wind turbine components "source NREL"14

Fig I.7 E-storage technologies improving their maturity level.....15

Fig I.8 Fuel cell Electrochemistry[9]16

Fig I.9 Algeria average of GHI 1994-2015.....18

Fig I.10 Annual maps of wind speed in Algeria at 10 m high [10]19

Fig II. 11 Project area location [12].....23

Fig II. 12 HOMER solver steps [13].....26

Fig II. 13: HOMER pro Interface[13].....27

Fig II. 14: HOMER main ribbon [13]27

Fig II. 15: location and time zone parameters28

Fig II. 16: Typical yearly profile of the solar radiation.....29

Fig II. 17: monthly average wind speed data30

**Fig II. 18: daily average temperature (source ‘office national de la meteorologie’
Ourgla-Algeria office).....30**

Fig II. 19 example of a constant daily load profile.....31

Fig II. 20: Daily load profile of the cell site32

Fig II. 21: Seasonal profile electric load32

Fig II. 22: Implementation of the stand-alone system.....	33
Fig II. 23: temperature effect parameters	35
Fig III. 24 Equivalent Circuit of Solar PV Cell [14].....	38
Fig III. 25 Variation of I-V Characteristic Curve of PV Cell with Categories of Different Losses [19]	42
Fig III .26 Orientation and Slope of Solar PV Module [22].....	47
Fig III. 27 Characteristic Curve of Typical Wind Turbine [24]	54
Fig III. 28 HOMER exemple of wind turbine power*wind speed curve [13]..	57
Fig IV. 29 optimum proposed system(categorized mode).....	62
Fig IV. 30 system ranked in tabular mode	63
Fig IV. 31 system schematic	64
Fig IV. 32 Fuel cell gen Dmap.....	67
Fig IV. 33 PV modules Dmap.....	68
Fig IV. 34 Wind turbine Dmap.....	69
Fig IV. 35 Electrolyzer Dmap	71
Fig IV. 36 Hydrogen tank Dmap	72
Fig IV. 37 Project cost summary	74
Fig IV. 38 diesel genset Dmap output	75
Fig IV. 39 cost summary.....	76

List of Tables

Table II. 1 Load profile table	25
Table II. 2 Variable power sources	33
Table II. 3 Storage system	33
Table II. 4 components costs	34
Table II. 5 Optimization capacity inputs	35
Table IV. 1 system architecture	64
Table IV. 2 Fuel Cell Summary	66
Table IV. 3 Generic flat plate PV Summary :	68
Table IV. 4 Generic 1 kW Summary	69
Table IV. 5 electrolyzer summary	70
Table IV. 6 Hydrogen Tank Properties	71
Table IV. 7 hydrogen Consumption Statistics	72
Table IV. 8 excess and unmet energy	72
Table IV. 9 Production Summary	73
Table IV. 10 project NPC costs	74
Table IV. 11 Net Present Costs	76
Table 1 split-type DC Variable frequency Air Conditioner SP4D technical specifications [27]	98

ACKNOWLEDGEMENT

First and foremost, praises and thanks to the God, the Almighty, for His showers of blessings throughout our thesis to complete it successfully.

I am extremely grateful to my parents for their love, prayers, caring and sacrifices for educating and preparing me for my future.

We would like to express our deep and sincere gratitude to our research supervisor, Dr. DERNOUNI Mhammed, Professor , renewable energies department for giving us the opportunity to do new research and providing invaluable guidance throughout this thesis.

He has taught us the methodology to carry out the research and to present the research works as clearly as possible. It was a great privilege and honor to work and study under his guidance, Also we express our thanks to our friends.

Finally, our thanks go to all the people who have supported us to complete the research work directly or indirectly.

MAATALLAH Sibaouih & DAHADJ Abdelghani

Nomenclature

CC	Cycle charging
COE	Cost of Energy
Dmap	(data map) is a type of graph showing one year of time series data. With time of day on one axis and day of the year on the other, each time step of the year is represented by a rectangle which is colored according to the data value for that hour.(from homer user manuel)
ea.	each
E	Equation of time [hr]
F	The cloudiness index
G	Solar irradiance [W/m^2]
HOMER	Hybrid Optimization Model for Electric Renewable
K	Boltzmann's constant [J/k]
P	Power available in the wind [kW]
Q	Electron charge [C]
UI	Overall heat loss (W/m^2)
E	the equation of time [hr]
LF	Load following
$T_{c,STC}$	the PV cell temperature under standard test conditions [$25\text{ }^\circ\text{C}$]
T_c	the PV cell temperature in the current time step [$^\circ\text{C}$]
Gen	Generator
IEA	international energy organization
NPC	Net present cost
NREL	National Renewable Energy Laboratory
PEMFC	Proton exchange membrane fuel cell
PV	Photovoltaic
$P_{v,oc}$	Open circuit temperature coefficient [Vov/k]
$T_{c,ref}$	PV cell temperature at standard conditions [k]
T_c	PV cell temperature [k]
T_r	PV cell reference temperature [k]
V_{mp}	PV maximum potential voltage [V]
$V_{mp.ref}$	Potential voltage at standard condition [V]
Q	Electron charge = $1.6 \cdot 10^{-19}$ [C]
T_a	Site ambient temperature [k]
H	Generator efficiency [%]
η_g	Electrical generator efficiencies [%]
η_m	The mechanical (gear box) [%]
f_{PV}	PV derating factor [%]
η_{pt}	tracking system efficiency [%]
η_r	Reference efficiency [%]
z_0	the surface roughness length [m]
\bar{G}_0	the extraterrestrial horizontal radiation averaged over the time step [kW/m^2]
\bar{G}_{0n}	the extraterrestrial normal radiation [kW/m^2]
CVP	Concentrated photovoltaic panels

HCVP	High concentrated photovoltaic panels
\bar{G}_T	the solar radiation incident on the PV array in the current time step [kW/m ²]
$\bar{G}_{T,STC}$	the incident radiation at standard test conditions [1 kW/m ²]
\bar{G}_b	the beam radiation [kW/m ²]
\bar{G}_d	the diffuse radiation [kW/m ²]
A_m	Area of single module (m ²)
G_o	Solar irradiance at standard test condition [kW/m ²]
G_t	Global radiation (W/m ²)
$I_{mp.ref}$	PV panels maximum current at standard conditions [A]
$I_{sc.ref}$	PV panels short circuit current at standard condition [A]
P_{pv}	Solar PV power output [W]
I_L	solar generated current [A]
I_o	Reverse saturation current of diode [A]
I_{sc,G_o}	Short circuit current at standard test condition [A]
I_{sc}	Short circuit current [A]
I_{sh}	Shunt-leakage current [A]
C_p	Fraction of wind power extracted by the wind rotor [%]
\bar{G}	the global horizontal radiation on the earth's surface averaged over the time step [kW/m ²]
\bar{G}_{0n}	is the extraterrestrial horizontal radiation averaged over the time step [kW/m ²]
G_{sc}	the solar constant [1.367 kW/m ²]
H_{ave}	the monthly average radiation on the horizontal surface of the earth [kWh/m ² /day]
$H_{o,ave}$	the extraterrestrial horizontal radiation, meaning the radiation on a horizontal surface at the top of the earth's atmosphere [kWh/m ² /day]
$P_{WTG,STP}$	the wind turbine power output at standard temperature and pressure [kW]
P_{WTG}	the wind turbine power output [kW]
P_{el}	wind turbine electrical power [kW]
U_{hub}	the wind speed at the hub height of the wind turbine [m/s]
U_{hub}	the wind speed at the hub height of the wind turbine [m/s]
U_{anem}	the wind speed at anemometer height [m/s]
U_{anem}	the wind speed at anemometer height [m/s]
Z_c	the time zone in hours east of GMT [hr]
t_c	the civil time in hours corresponding to the midpoint of the time step [hr]
t_s	the solar time [hr]
z_{hub}	the hub height of the wind turbine [m]
z_{hub}	the hub height of the wind turbine [m]
z_{anem}	the anemometer height [m]
z_{anem}	the anemometer height [m]
IRENA	International Renewable Energy Agency
Erg	unit of energy or work in the centimeter-gram-sec system of physical units =10 ⁻⁷ Joule
CVP	Concentrated photovoltaic
TFSC	Thin-Film Solar Cells
CdTe	Cadmium Telluride Solar Cell
E_{Nernst}	the thermodynamic equilibrium potential or open circuit voltage
ea.	each

GREEK LETTERS

β_t	Temperature coefficient efficiency ranging from 0.004 to 0.006/°C for silicon cells.
ω_1	the hour angle at the beginning of the time step [°]
ω_2	the hour angle at the end of the time step [°]
θ_z	the zenith angle [°]
α_p	the temperature coefficient of power [%/°C]
δ	the solar declination [°]
λ	is the longitude [°]
ω	is the hour angle [°]
ϕ	is the latitude [°]
η_{act}	Activation overvoltage
η_{ohmic}	Ohmic overvoltage
η_{conc}	concentration overvoltage

INTRODUCTION

Introduction:

The science of electricity was pioneered in the 18th and early 19th centuries by luminaries such as Franklin, Faraday, Volta, Ampere, Ohm and Maxwell. They laid the foundation for the second industrial revolution in the late 19th century, which was enabled by the engineering of such resonant names as Edison, Bell, Tesla and Westinghouse, whose inventions spanned from light bulbs to electric railways and industrial electric machines [1].

Nowadays, electricity energy became a main part of our life due to its contribution in serving a wide range of sectors such as lightning , communications ,refrigeration/warming ,lighting ,and many other essential power systems .

However ,currently ,according to IEA [2]estimation 1.1 billion people (14% of global population) didn't have access to electricity Around 84% of those without electricity access reside in rural areas and more than 95% of those living without electricity are in countries in sub-Saharan Africa and developing Asia .

Although even if the excess to electricity exist its quality is an important factor as well, according to the same reference further one billion suffer from poor quality electrical energy , to minimize this problems off-grid systems was created, this systems could come with multiple sizes such as micro or ever nano grids also they have many names such as standalone ,autonomous or remote area power supply (RAPS) but they all have the a common objective which is to ensure supply and distribution electrical system, The term nanogrid, originated by Lawrence Berkeley National Laboratory is defind by The World Bank as:

Isolated, small-scale distribution networks typically operating below 11 kilovolts (kV) that provide power to a localized group of customers and produce electricity from small generators, potentially coupled with energy storage system [3].

These systems include different way of generation, storing and controlling power systems For the generating process they either based traditional fossil sources or renewable sources

for the backup need they might be rely on batteries, flywheels or ever fuel cells,for the controlling purposes they may use some optimized dispatch controller to reduce loses.

Systems that combined more than one power supply are usually called Hybrid Systems, these system solved a lot of electrical grid lack access issues.

Although this hybrid systems may include some dirty and exhausted sources such as diesel, gas, coal that the most ranked in term of pollution and carbon dioxide emissions ,the renewable power sources are usually clean and less air polluted produce air pollution, but they rely on variable sources which cause a energy stability problems

On this thesis our objective is to provide an optimal design for a hybrid power system for remote area that overcomes all the above problems.

We've divided our thesis into four chapters :

On the first chapter we viewed a literature review about the off-grid systems and their improvements, we also talked about the Algerian potential renewable resources .

On the seconde chapter we described our load and the used method to design our hybrid renewable system which based on HOMER pro software.

On the third chapter we modeled our power system components by defining the most important relations to calculate the power output from the system inputs.

On the fourth chapter we displayed our results and their discussions.

Finally we end by a brief summary of the conclusions and we provided our outlooks.

CHAPTER I

Chapter I: Literature Review

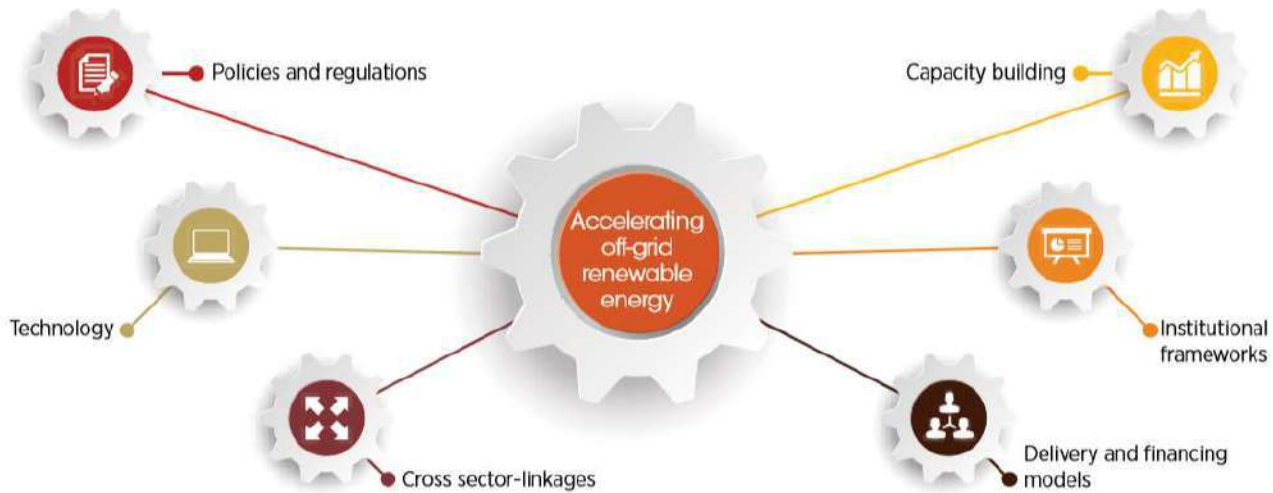
I.1 Introduction:

The 2030 Agenda for Sustainable Development positions access to affordable, reliable, sustainable and modern energy as a key pillar of Sustainable Development Goal 7 (SDG 7) (UN, 2018). This represents a growing recognition that modern energy is a key building block towards broader development goals associated with environmental sustainability, delivery of public services and poverty eradication. Access to reliable and affordable electricity, for example, can have an immediate and transformative impact on quality of life, access to basic services (e.g., health, education) and livelihoods [4].

I.2 Bibliographic review:

Off-grid renewable energy solutions have emerged as a mainstream solution to expand access to modern energy services in a timely and environmentally sustainable manner. Over the past five years, the deployment of stand-alone and minigrid systems has witnessed tremendous progress as technology costs have plummeted, innovation in deployment and financing models has picked up, and a more diverse set of stakeholders, including local entrepreneurs, the international private sector and financing institutions, have become engaged in the sector. Besides providing energy for lighting and cooking, off-grid solutions are being deployed to support the delivery of public services (e.g., education, water and primary health care), the development of livelihoods by powering productive end-uses (e.g., agriculture) and other commercial and industrial needs [4].

The evidence base on the transformative socioeconomic impact of off-grid solutions is expanding with the documentation of country- and project level case studies. A more complete picture on the status and trends of off-grid renewable energy technologies requires addressing challenges associated with the availability of, and accessibility to, harmonized data at the national and regional levels. Efforts are also needed to address other methodological challenges such as the definition and categorization of off-grid renewable energy systems [4].



Source: IRENA, 2017b

Fig I.1 The enabling environment for scaling up off-grid solutions

The number of people served by off-grid renewables globally has expanded six-fold since 2011, reaching nearly 133 million people in 2016 [4].

IRENA¹ estimates that some 133 million people accessed lighting and other electricity services using off-grid renewable energy solutions in 2016. This includes about 100 million using solar lights (<11 watts), 24 million using solar home systems (>11 watts) and at least 9 million connected to a mini-grid. A large part of the growth in off-grid renewables has occurred over the last five years, driven by the rapidly decreasing costs of solar lighting solutions and by the establishment of local supply chains making these solutions accessible. The adoption of innovative delivery and tailored financing models, such as pay-as-you-go (PAYG) and micro-financing, has driven the growth of solar home systems that offer a wider range of electricity services [4].

Off-grid renewable energy capacity has witnessed a spectacular three-fold increase from under 2 gigawatts (GW) in 2008 to over 6.5 GW in 2017. While a proportion of the deployed capacity is to support household electrification, a majority (83%) is dedicated for industrial (e.g., co-generation), commercial (e.g., powering telecommunication infrastructure) and public end-uses (e.g., street lighting, water pumping) [4].

CHAPTER I : LITERATURE REVIEW

Developments in off-grid renewable energy vary across regions. Countries in Africa and Asia account for most of the growth over the past years, with more than 53 million people in Africa and 76 million in Asia now using such power sources [4].

Africa has emerged as a dynamic, fast moving hub for off-grid renewables

The African continent has seen rapid developments in off-grid renewable energy over the past five years. The population served by off-grid solutions in Africa grew rapidly from just over 2 million people in 2011 to over 53 million in 2016.

Solar lights have driven this rapid growth, but about 10% of the population served in Africa (5.4 million) obtained a higher level of electricity services from off-grid solar (Tier 1 access or more).

Solar home systems reached over 4 million people in 2017.

The cumulative off-grid renewable energy capacity has increased from 231 megawatts (MW) in 2008 to nearly 1.2 GW in 2017. The deployment of solar technologies has been a key driver of growth in off-grid capacity, with over 820 MW installed as solar lights, home systems and mini-grids and for commercial/public services. The abundance of the resource, the distributed nature of technology and decreasing costs are leading solar to become a default choice for meeting a wide range of electricity services in areas largely underserved by the national grid [4].

The capacity of hydropower-based mini-grids has grown from 124 MW in 2008 to 162 MW in 2017, although its share in total off-grid capacity fell from 53% to under 15% during the same period. Besides electrification, off-grid capacity for self consumption in industry has grown (e.g., bagassebased co-generation) from 29 MW in 2008 to nearly 200 MW in 2017.

I.3 Power sources definitions:

I.3.1 Solar power:

Solar radiation, electromagnetic radiation, including X-rays, ultraviolet and infrared radiation, and radio emissions, as well as visible light, emanating from the Sun. Of the

3.8×10^{33} ergs emitted by the Sun every second, about 1 part in 120 million is received by its attendant planets and their satellites. The small part of this energy intercepted by Earth (the solar constant, on average 1.4 kilowatts per square meter) is of enormous importance to life and to the maintenance of natural processes on Earth's surface.

The energy output of the Sun has its peak at a wavelength of 0.47 micrometer (0.000019 inch; a micrometer is 10^{-6} meter), and the Sun radiates about 8 kilowatts per square cm of its surface [5].

Different types of solar panels serve different needs and purposes

Given that sunlight can be used differently whether on Earth or in space points to the fact that location, itself, is a significant factor when it comes to choosing one of the types of solar panels over another.

Distinguishing between different types of solar panels often means differentiating between single-junction and multi-junctions solar panels or first, second, or third generations. Single-junction and multi-junctions differ in the number of layers on the solar panel that will observe the sunlight, whereas the classification by generation focuses on the materials and efficiency of the different types of solar panels [6].

I.3.1.1 First Generation Solar Panels

These are the traditional types of solar panels made of monocrystalline silicon or polysilicon and are most commonly used in conventional surroundings.

I.3.1.1.1 Monocrystalline Solar Panels (Mono-SI)

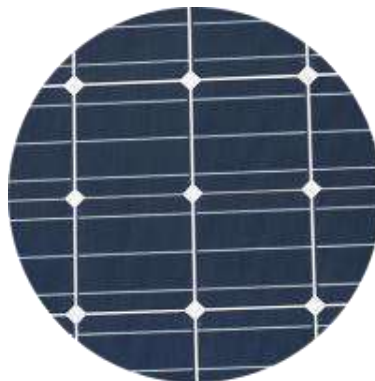


Fig I.2 Monocrystalline Solar Panels (Mono-SI) [6]

This type of solar panels (made of monocrystalline silicon) is the purest one. You can easily recognize them from the uniform dark look and the rounded edges. The silicon's high purity causes this type of solar panel has one of the highest efficiency rates, with the newest ones reaching above 20% [6].

Monocrystalline panels have a high power output, occupy less space, and last the longest. Of course, that also means they are the most expensive of the bunch. Another advantage to consider is that they tend to be slightly less affected by high temperatures compared to polycrystalline panels [6].

I.3.1.1.2 Polycrystalline Solar Panels (Poly-SI)

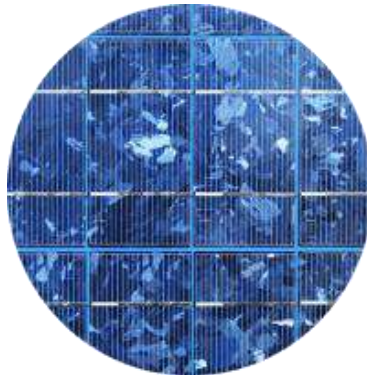


Fig I.3 Polycrystalline Solar Panels (Poly-SI) [6]

You can quickly distinguish these panels because this type of solar panels has squares, its angles are not cut, and it has a blue, speckled look. They are made by melting raw silicon, which is a faster and cheaper process than that used for monocrystalline panels [6].

This leads to a lower final price but also lower efficiency (around 15%), lower space efficiency, and a shorter lifespan since they are affected by hot temperatures to a greater degree. However, the differences between mono- and polycrystalline types of solar panels are not so significant and the choice will strongly depend on your specific situation. The first option offers a slightly higher space efficiency at a slightly higher price but power outputs are basically the same [6].

I.3.1.2 Second Generation Solar Panels:

These cells are different types of thin film solar cells and are mainly used for photovoltaic power stations, integrated in buildings or smaller solar power systems.

I.3.1.2.1 Thin-Film Solar Cells (TFSC):



Fig I.4 Thin-Film Solar Cells (TFSC) [6]

If you are looking for a less expensive option, you might want to look into thin-film. Thin-film solar panels are manufactured by placing one or more films of photovoltaic material (such as silicon, cadmium or copper) onto a substrate. These types of solar panels are the easiest to produce and economies of scale make them cheaper than the alternatives due to less material being needed for its production[6].

They are also flexible which opens a lot of opportunities for alternative applications and is less affected by high temperatures. The main issue is that they take up a lot of space, generally making them unsuitable for residential installations. Moreover, they carry the shortest warranties because their lifespan is shorter than the mono- and polycrystalline types of solar panels. However, they can be a good option to choose among the different types of solar panels where a lot of space is available[6].

I.3.1.3 3rd Generation Solar Panels(3):

3rd generation solar panels include a variety of thin film technologies but most of them are still in the research or development phase. Some of them generate electricity by using organic materials, others use inorganic substances (CdTe for instance).

I.3.1.3.1 Biohybrid Solar Cell:

The Biohybrid solar cell is one of the types of solar panels, that is still in the research phase. It has been discovered by an expert team at Vanderbilt University. The idea behind the new technology is to take advantage of the photosystem 1 and thus emulate the natural process of photosynthesis. In case you want to learn more about how the biohybrid solar cell works in detail, read more about it in the American Journal of Optics and Photonics. It explains more detailed how these cells work. Many of the materials being used in this cell are similar to the traditional methods, but only by combining the multiple layers of photosystem 1, the conversion from chemical to electrical energy becomes much more effective (up to 1000 times more efficient than 1st generation types of solar panels) [6].

I.3.1.3.2 Cadmium Telluride Solar Cell (CdTe)

Among the collection of different types of solar panels, this photovoltaic technique uses Cadmium Telluride, which enables the production of solar cells at relatively low cost and thus a shorter payback time (less than a year). Of all solar energy technologies, this is the one requiring the least amount of water for production. Keeping the short energy payback time in mind, CdTe solar cells will keep your carbon footprint as low as possible. The only disadvantage of using Cadmium Telluride is its characteristic of being **toxic**, if ingested or inhaled. In Europe especially, this is one of the greatest barriers to overcome, as many people are very concerned about using the technology behind this type of solar panel [6].

I.3.1.3.3 Concentrated PV Cell (CVP and HCVP)

Concentrated PV cells generate electrical energy just as conventional photovoltaic systems do. Those multi-junction types of solar panels have an efficiency rate up to 41%, which, among all photovoltaic systems, is the highest so far.



Fig I.5 Concentrated PV Cell (CVP and HCVP) [6]

The name of such CVP cells is related to what makes them so efficient, compared to other types of solar panels: curved mirror surfaces, lenses and sometimes even cooling systems are used to bundle the sun rays and thus increase their efficiency.

By this means, CVP cells have become one of the most efficient types of solar panels, with a high performance and efficiency rate of up to 41%. What remains is the fact, that such CVP solar panels can only be as efficient if they face the sun in a perfect angle. In order to reach such high efficiency rates, a solar tracker inside the solar panel is responsible for following the sun [6].

I.3.2 Wind Energy and Wind Power

Caused by the uneven heating of the atmosphere by the sun, the irregularities of the earth's surface, and rotation of the earth. Wind flow patterns are modified by the earth's terrain, bodies of water, and vegetative cover. This wind flow, or motion energy, when "harvested" by modern wind turbines, can be used to generate electricity [7].

How Wind Power Is Generated

The terms "wind energy" or "wind power" describe the process by which the wind is used to generate mechanical power or electricity. Wind turbines convert the kinetic energy in the wind into mechanical power. This mechanical power can be used for specific tasks (such as

grinding grain or pumping water) or a generator can convert this mechanical power into electricity to power homes, businesses, schools, and the like [7].

I.3.2.1 Wind Turbines :

Wind turbines, like aircraft propeller blades, turn in the moving air and power an electric generator that supplies an electric current. Simply stated, a wind turbine is the opposite of a fan. Instead of using electricity to make wind, like a fan, wind turbines use wind to make electricity. The wind turns the blades, which spin a shaft, which connects to a generator and makes electricity [7].

I.3.2.1.1 Wind Turbine Types:

Modern wind turbines fall into two basic groups:

the horizontal-axis variety, like the traditional farm windmills used for pumping water,

the **vertical-axis** design, like the eggbeater-style Darrieus model, named after its French inventor. Most large modern wind turbines are horizontal-axis turbines.

I.3.2.1.2 Turbine Components

Horizontal turbine components include:

blade or rotor, which converts the energy in the wind to rotational shaft energy, a drive train, usually including a gearbox and a generator, a tower that supports the rotor and drive train; and other equipment, including controls, electrical cables, ground support equipment, and interconnection equipment [7].

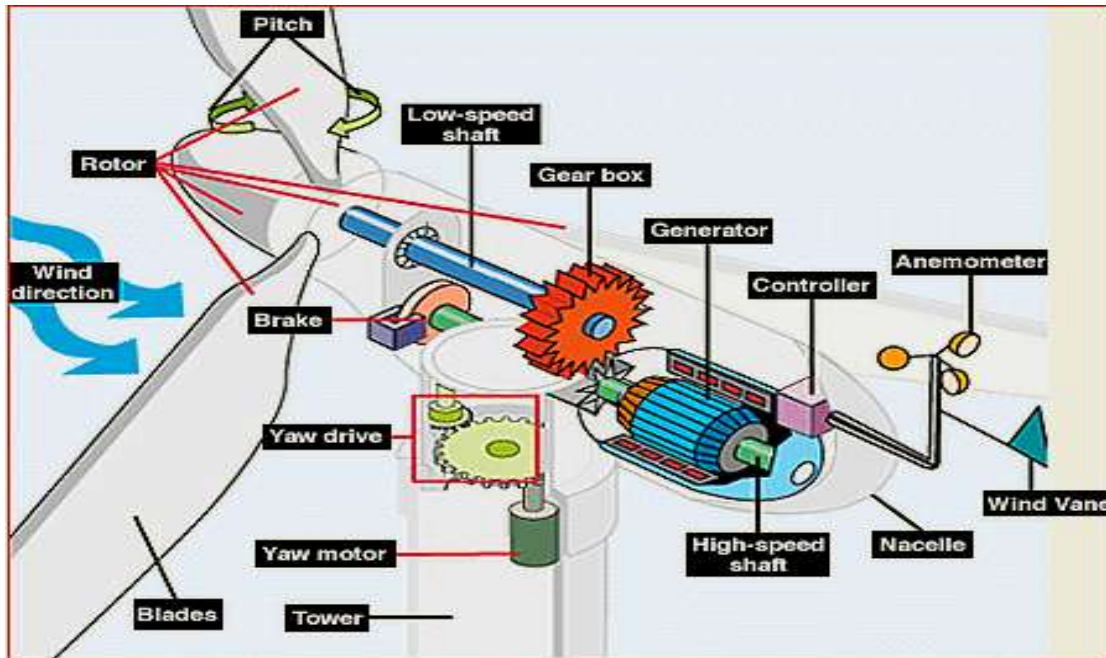


Fig I.6 horizontal Wind turbine components "source NREL"

I.3.2.1.3 Turbine Configurations:

Wind turbines are often grouped together into a single wind power plant, also known as a wind farm, and generate bulk electrical power. Electricity from these turbines is fed into a utility grid and distributed to customers, just as with conventional power plants [7].

I.3.3 Storage system

I.3.3.1 Power-to-gas conversion:

Power-to-gas is a storage solution that can help address grid-stability problems that arise when an increasing share of power is generated from sources that have a highly variable output. The technology is undergoing advanced study and approaching commercial application. A power-to-gas system converts electricity generated during periods of high output and low demand (such as strong wind during off-peak hours) by splitting water molecules into hydrogen and oxygen through electrolysis. The hydrogen is stored for future use as fuel and the oxygen may be sold for industrial use or released into the atmosphere [8].

There are three potential uses for the stored hydrogen:

- a. Using hydrogen gas blended with natural gas, or directly, in applications such as power generation or transport fuel

CHAPTER I : LITERATURE REVIEW

- b. Feeding fuel cells by injecting hydrogen and oxygen (or air) into the cell to produce a chemical reaction and as a result electricity
- c. Combining the hydrogen with carbon dioxide to create synthetic methane, which could be used as an alternative to natural gas

The commercial use of power-to-gas technology is primarily being considered in Europe, where it is being reviewed by the European Gas Research Group, as well as the energy departments of several countries. Germany is leading the way, with 18 different experimental programs in progress. Power-to-gas conversion technology is also being evaluated for commercial application in the US by the Southern California Gas Company, in conjunction with the U.S. Department of Energy's National Renewable Energy Laboratory and the National Fuel Cell Research Center at the University of California, Irvine.¹⁶ [8].

The figure 3 show us that the hydrogen storage technique is still under research and development process and we can see also that it has a cost that is relatively low.

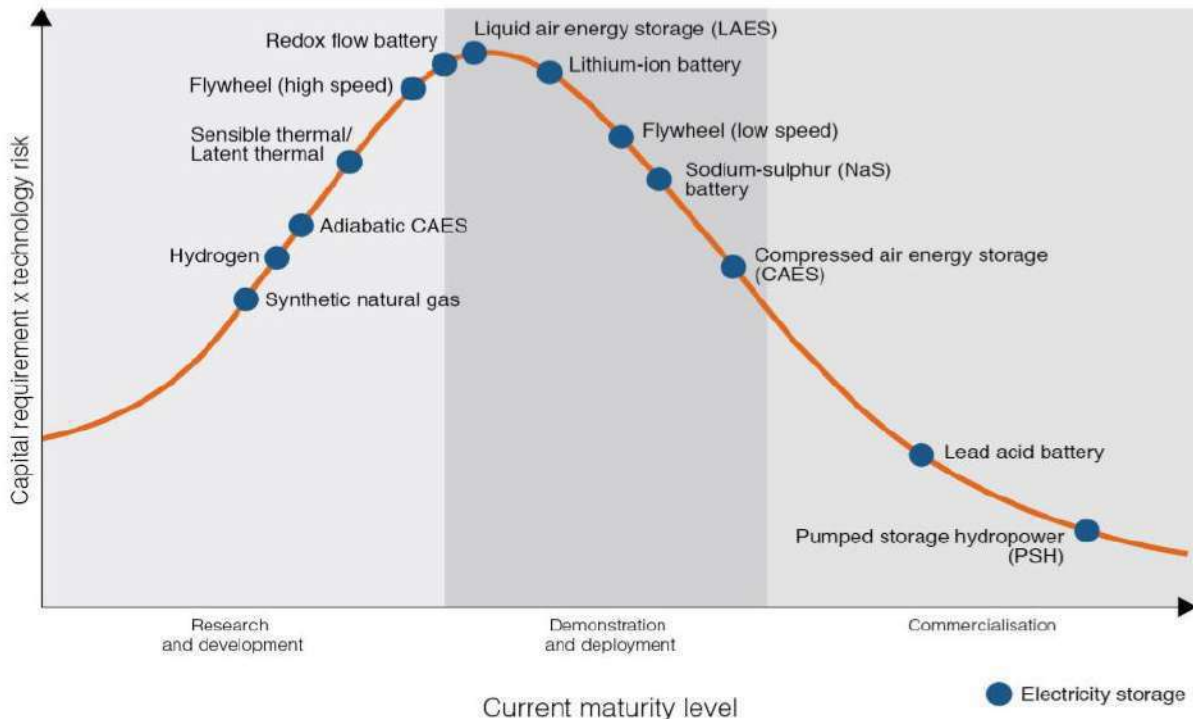
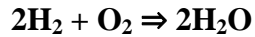


Fig I.7 E-storage technologies improving their maturity level

I.3.3.1.1 Proton Exchange Membrane (PEM) Fuel Cell :

The most common fuel cells use Hydrogen as the fuel and Oxygen from the air as the oxidant. The basic reaction can be illustrated by the Proton Exchange Membrane (PEM) fuel cell. (Also called the Polymer Electrolyte Membrane fuel cell [9].

The overall equation for the reaction is:



The equation for the reactions at the individual electrodes is shown where they take place on the diagram below (fig I.8).

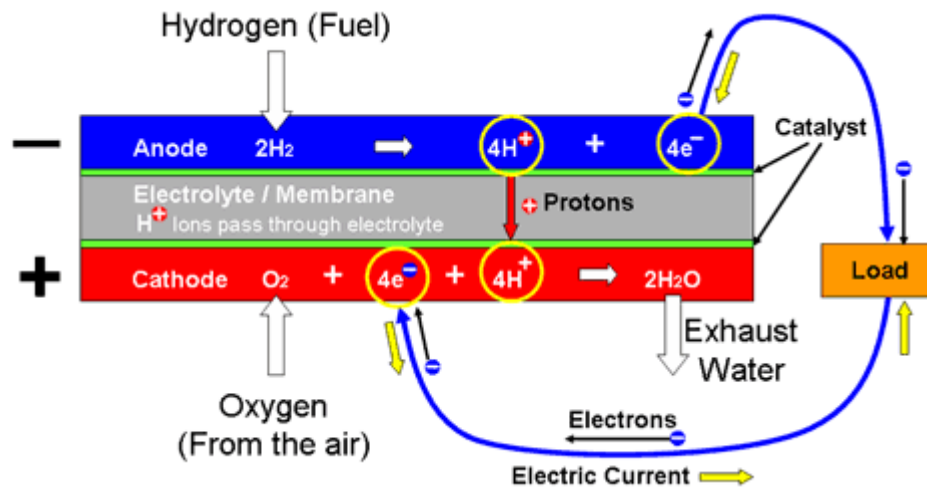


Fig I.8 Fuel cell Electrochemistry[9]

I.4 Potential and applications of renewable energy in Algeria

Algeria plays a key role in world energy markets as a leading producer and exporter of natural gas and liquefied natural gas. Algeria's energy mix in 2010 was almost exclusively based on fossil fuels, especially natural gas (93%). However the country has enormous renewable energy potential, mainly solar, which the government is trying to harness by launching an ambitious Renewable Energy and Energy Efficiency Program.

The Program consists of generating 22,000 MW of power from renewable sources between 2011 and 2030, of which 12,000 MW will be meant for domestic consumption and the rest for export. The Program is focused on developing and expanding the use of renewable resources, such as solar, wind, biomass, geothermal and hydropower, in order to diversify energy sources and promote sustainable development of the country [10].

Around 60 solar photovoltaic plants, concentrating solar power plants, wind farms as well as hybrid power plants are to be constructed within the next ten years. Algeria has also joined the 'Desertec' Industrial Initiative, which aims to use Sahara solar and wind power to supply 15 per cent of Europe's electricity needs by 2050 [10].

I.4.1 Solar Energy:

The country receives annual sunshine exposure equivalent to 2,500 KWh/m². Daily solar energy potential varies from 4.66 kWh/m² in the north to 7.26 kWh/m² in the south.

Pilot projects for the construction of two solar power plants with storage of a total capacity of about 150 MW each, will be launched during the 2011-2013 period. These will be in addition to the hybrid power plant project of Hassi R'Mel with a total power capacity of 150 MW, including 25 MW in solar. Four solar thermal power plants with a total capacity of about 1,200 MW are to be constructed over the period of 2016 to 2020 [11].

The Hassi R'Mel integrated solar combined cycle power station is one of world's first hybrid power stations. The plant combines a 25 MW parabolic trough concentrating solar power array, covering an area of over 180,000 m², in conjunction with a 130 MW combined cycle gas turbine plant, so cutting carbon emissions compared to a traditional power station. The gas turbine and steam cycle are fired by natural gas, with the steam turbine receiving additional solar-generated steam during the day. The plant began electricity production in June 2011 [11].

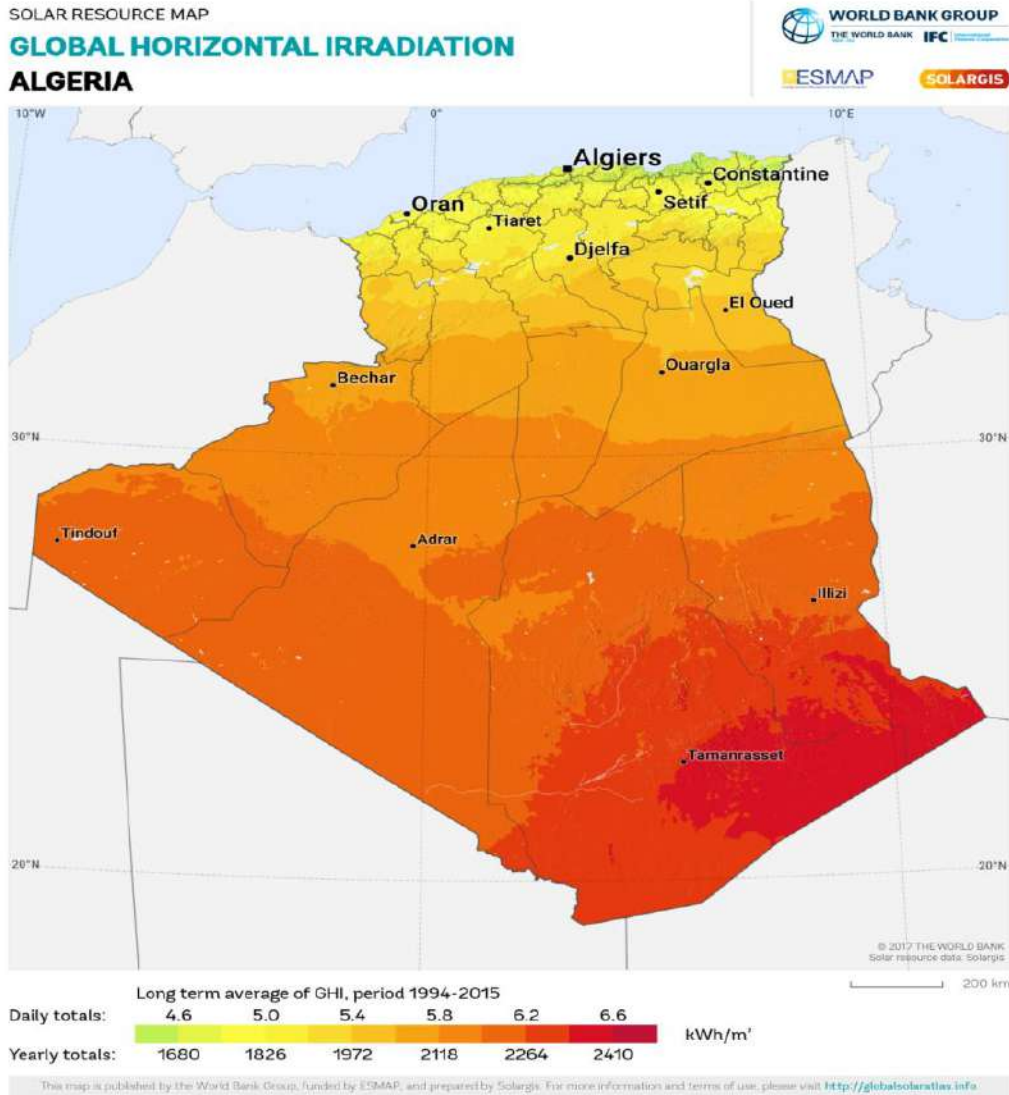


Fig I.9 Algeria average of GHI 1994-2015

I.4.2 Wind Energy:

Algeria has promising wind energy potential of about 35 TWh/year. Almost half of the country experience significant wind speed. The country's first wind farm is being built at Adrar with installed capacity of 10MW with substantial funding from state-utility Sonelgaz. Two more wind farms, each of 20 MW, are to be developed during 2014- 2013. Studies will be led to detect suitable sites to realize the other projects during the period 2016-2030 for a power of about 1700 MW [11].

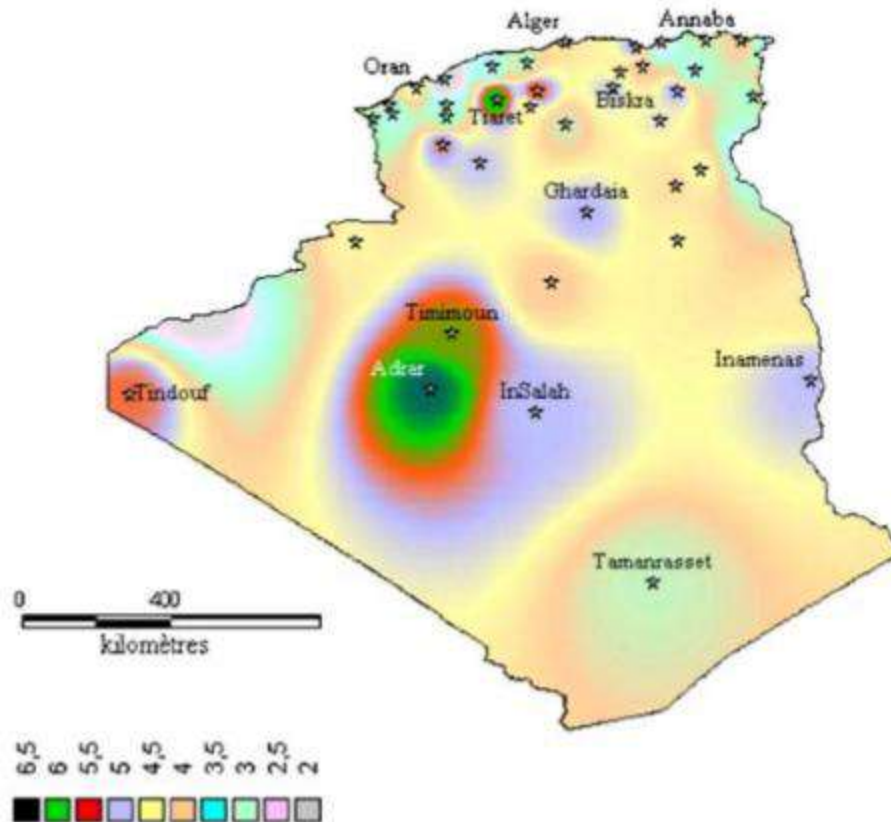


Fig I.10 Annual maps of wind speed in Algeria at 10 m high [10]

I.4.2.1 Wind map of Algeria

Algeria is generally quite windy. 78% of its surface is characterized by velocities exceeding 3 m/s with about 40% of these speeds are above 5 m/s. Wind maps show that the highest wind speeds are distributed in the south while the north is generally less windy. It was found also that the southwestern region has a great potential with speeds exceeding 4 m/s for the site of Bechar, 5 m/s for the site of Tindouf and even above 6 m/s for the site of Adrar. The fact the southwestern region of the country has a significant wind potential can be attributed to two factors:

- a. The first is that it is located in an area of pressure difference (wind in the latitudes near 30°N).
- b. The second is that it is close to the Atlantic Ocean (weather disturbances reaches the region with high intensity).

CHAPTER I : LITERATURE REVIEW

On the other hand, in southeastern part of the country, it has been found that the wind potential is relatively weaker with respect to the western part. The highest speeds of 4.5 m/s were observed for the region Inamenass.

So for the Tamanrasset region, we observe that the wind potential is below 4 m/s. taking into account the topographical aspect, the decrease of wind potential in this region can be attributed to the mountains series of Tassili which distracts and prevents some weather disturbances to reach the region. Concerning the site of Hassi-R'mel, Table 1 indicates that it has a very significant wind potential ($v \approx 6$ m/s).

We can see that the wind in Algeria obeys the same monthly rules.

Monthly velocities vary a little. Taking into account such results, this region is very favorable and adequate for the systems of wind energy conversion [10].

I.5 Chapter summary:

On this chapter we viewed the present state of standalone systems and their evolutions and development.

We also defined our system components, fundamentals and techniques behind their resources to power conversion

Finally we described the abundant of our system resources in Algeria.

CHAPTER II

Chapter II: Design and Optimization Method

II.1 Introduction:

Designing a renewable based energy system for a remote area with a traditional ways isn't reliable nowadays, because most of renewable sources are variable also the load demand depends on many factors despite the components energy consumption, for that reason we must work with a sophisticated tool to guarantee our system reliability.

Homer pro software is the one most known software on the globe for designing reliable renewable systems, it also an amazing tool for optimizing these systems , on this chapter we will talk about our system load type and we'll take an overview on how to use Homer pro to provide an optimum energy source to this load ?

II.2 Load background:

II.2.1 Case study:

“IFNI” village is a remote area in TASSILI N'AJZER national park located in the south-east of ILLIZI province, South-west of Algeria country, it gathers an amazing landscapes and a cool weather, and also it's a transit way to many other remote villages.

This village is occupied with a few number of people, the living condition of these people depends on shepherding and some agricultural activities.

The geographical location coordinates of the site are $25^{\circ}53, 3'N$ latitude and $7^{\circ}53.3'E$ longitudes

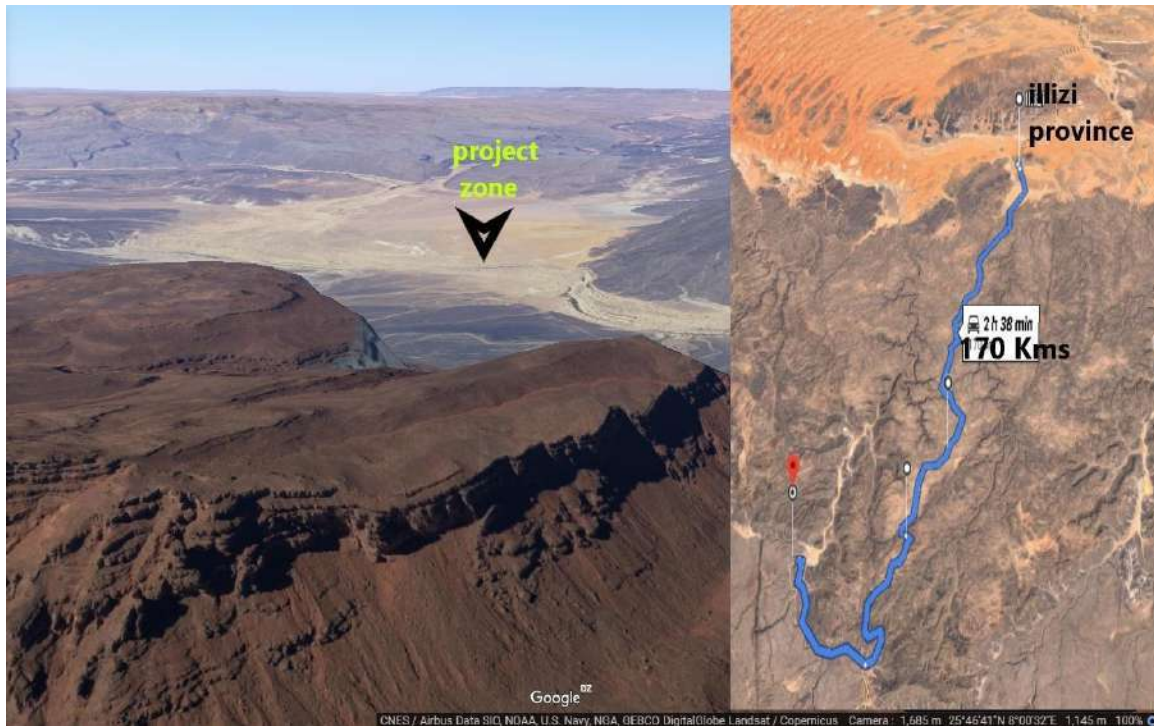


Fig II. 11 Project area location [12]

The aim of our study is to provide an optimal design of standalone hybrid renewable energy system for the electrification of a telecom cell site to provide a reliable telecommunication system for this village .

II.2.2 Load descriptions:

Primary load is the load that should meet by the energy provided by the system as it requires immediately; which includes lighting, baking, vaccine refrigeration, TV, radio, computer, printer, fax, simple laboratory equipment's and others.

In our study the primary load consist of a typical cell site or **base transceiver station** or **BTS**

II.2.2.1 BTS definition:

In Global System for Mobile Communications (GSM) networks, the correct term is Base Transceiver Station (BTS), and colloquial synonyms are "mobile phone mast" or "base station". Multiple cellular providers often save money by mounting their antennas on a common shared mast; since separate systems use different frequencies, antennas can be located close together without interfering with each other. Some provider companies operate multiple cellular networks

and similarly use collocated base stations for two or more cellular networks, (CDMA2000 or GSM, for example).

The power density P_d in a distance R of the radio wave from the BTS antenna is given by the following law

$$P_d = \frac{P_t G}{4\pi R^2} \text{ (Watt/m}^2\text{)} \quad \text{(II-1)}$$

Where P_t transmitter power in watt

G Gain of transmitten antenna

R distance from the antenna in m

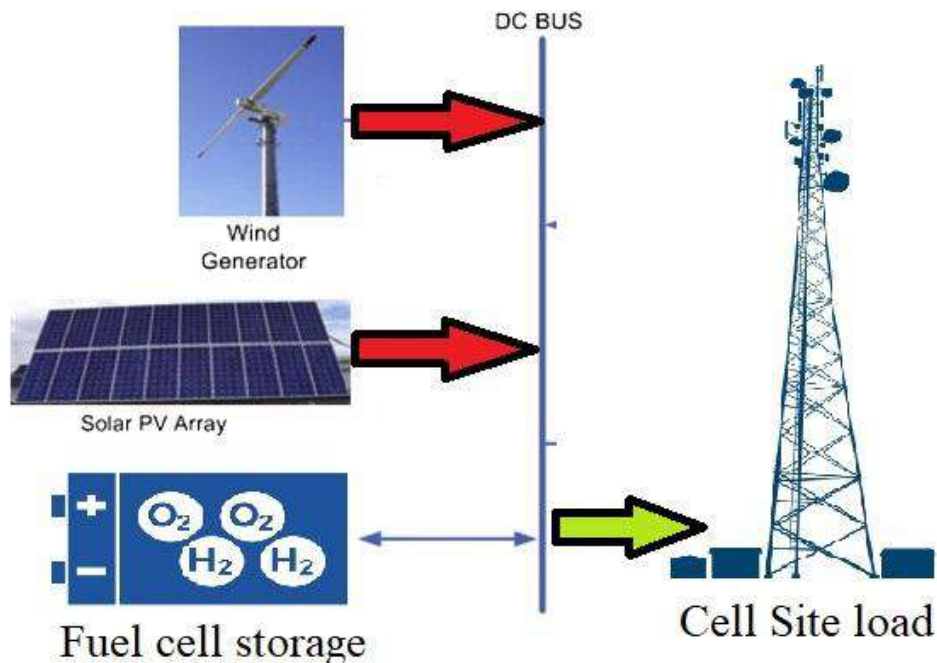


Fig II.12 Proposed system schematic

II.2.2.1.1 Load profile calculation:

Here the electricity load consumption of the cell site considered to be the same and constant throughout the year except the summer period where the temperature increases (more cooling power needed).

The load determination of the cell site was performed for a typical cell site and according to MOBILIS telecom company energy engineer helps ‘Mohammed Salah Hammadi’ .

The economic situation of the country isn’t so high and thus in this energy system design the selection of appliances was reflected for the low wattage for the affordability of the provided electric energy.

The primary load energy estimation is made according the following approach. :

$$E_t = \sum_{i=1}^n [P_i * R_i * 24] \quad (II-2)$$

Where : R_i : i rating of appliance

E_t :is total energy consumption

P_i :is i appliance used power

Table II. 1 Load profile table

Equipments	Quantity	Consumption{w}	Energy{w.h}	Volts	Amps
BTS	1	4752	114048	48	99
MICROWAVE ANTENNA	1	417.6	10022.4	48	8.7
DCAIR CONDITIONNER	1	935	22440	48	23
Total		6104.6	146510.4		

II.3 Methods and material

II.3.1 HOMER energy software:

HOMER (Hybrid Optimization of Multiple Electric Renewables), the micropower optimization model, simplifies the task of evaluating designs of both off-grid and grid-connected power systems for a variety of applications. When you design a power system, you must make

many decisions about the configuration of the system: what components does it make sense to include in the system design? How many and what size of each component should you use? The large number of technology options and the variation in technology costs and availability of energy resources make these decisions difficult. HOMER's optimization and sensitivity analysis algorithms make it easier to evaluate the many possible system configurations[13].

Working effectively with HOMER requires understanding of its three core capabilities - simulation, optimization, and sensitivity analysis - and how they interact [13].

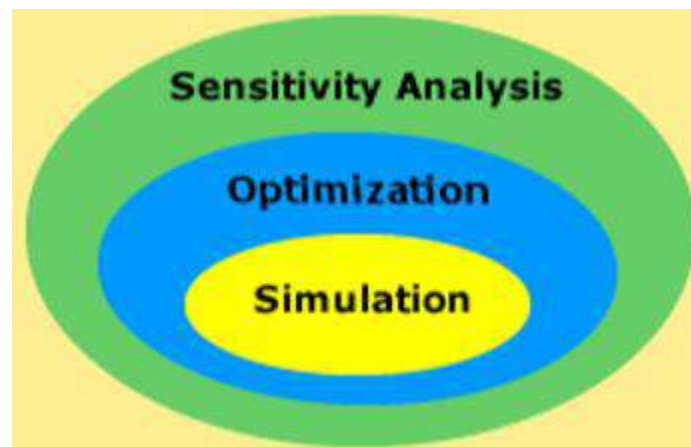


Fig II. 12 HOMER solver steps [13]

Simulation: At its core, HOMER is a simulation model. It will attempt to simulate a viable system for all possible combinations of the equipment that you wish to consider. Depending on how you set up your problem, HOMER may simulate hundreds or even thousands of systems [13].

Optimization: The optimization step follows all simulations. The simulated systems are sorted and filtered according to criteria that you define, so that you can see the best possible fits. Although HOMER fundamentally is an economic optimization model, you may also choose to minimize fuel usage [13].

Sensitivity analysis: This is an optional step that allows you to model the impact of variables that are beyond your control, such as wind speed, fuel costs, etc, and see how the optimal system changes with these variations [13].

HOMER models both conventional and renewable energy technologies

II.3.1.1 Interfaces of HOMER pro:

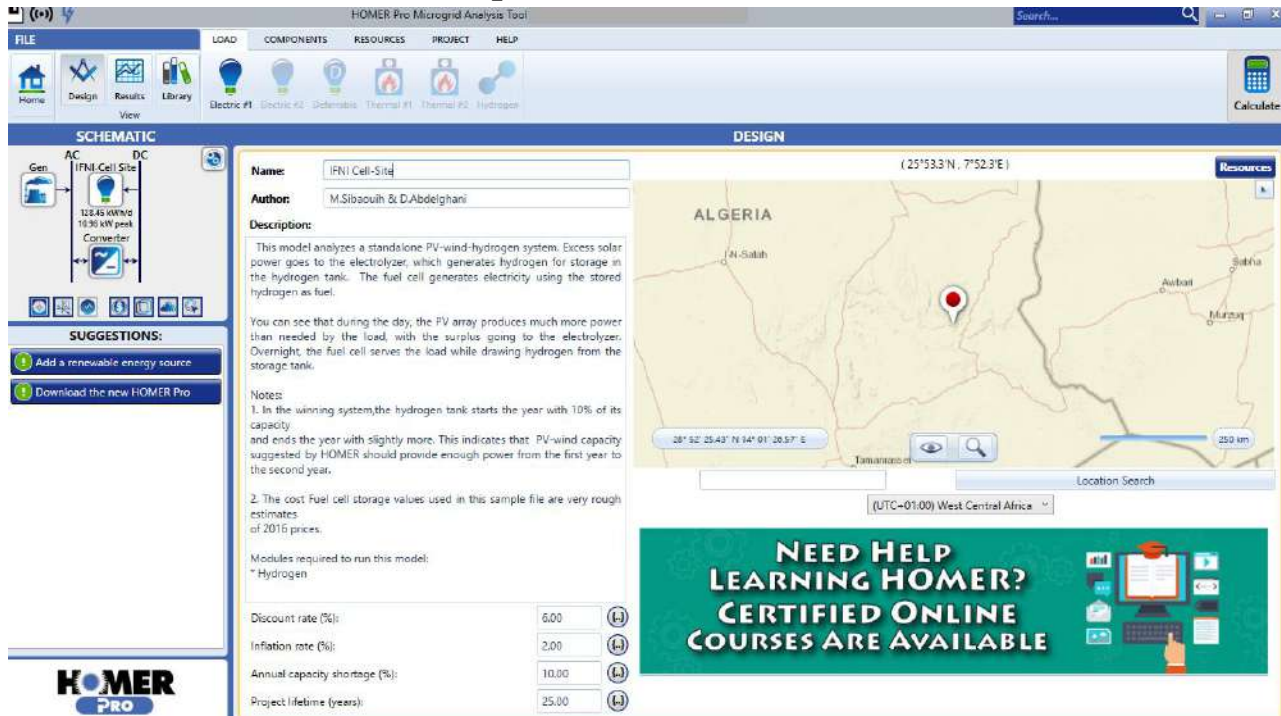


Fig II. 13: HOMER pro Interface[13]

II.3.1.2 Begin the project information inputs:

In order to use Homer pro software we need first to

Add a load by directly import a load profile time series file or use homer ready-to-use load examples (residential , commercial ,industrial ,community) or input the time series manually by choosing a bland yearly load data (for more see ‘load profile title’ II.3.1.2.2).

Next we add our system component (more details in ‘Choose components title’II.3.1.3).

Then we added the system needed resources (for more information on how to do that see ‘System resources title’II.3.1.2.1.1) .



Fig II. 14: HOMER main ribbon [13]

II.3.1.2.1 Project location input:

From the initial star-up screen globe map field we putted our geographical location coordinates on coordinate's box

The time zone is another parameter to be set. The village is located at latitude: 25°53.3'N latitude and 7°53.3'E longitudes, and with time zone of GMT +1:00.



Fig II. 15: location and time zone parameters

II.3.1.2.1.1 System resources:

In order to calculate how much power is generated by the solar PV inputting measured solar resources data in units of kW/m^2 into HOMER software is needed first, as mentioned in homer 'required changer' window.

II.3.1.2.1.1.1 Solar resource:

The solar global horizontal irradiation and the clearness index was downloaded from National renewable Energy Lab database, national solar radiation database under:

Cell number:413262 Cell demensions:40km x 40km

Cell midpointLatitude: 25.8 Cell midpoint Longitude:8.164226

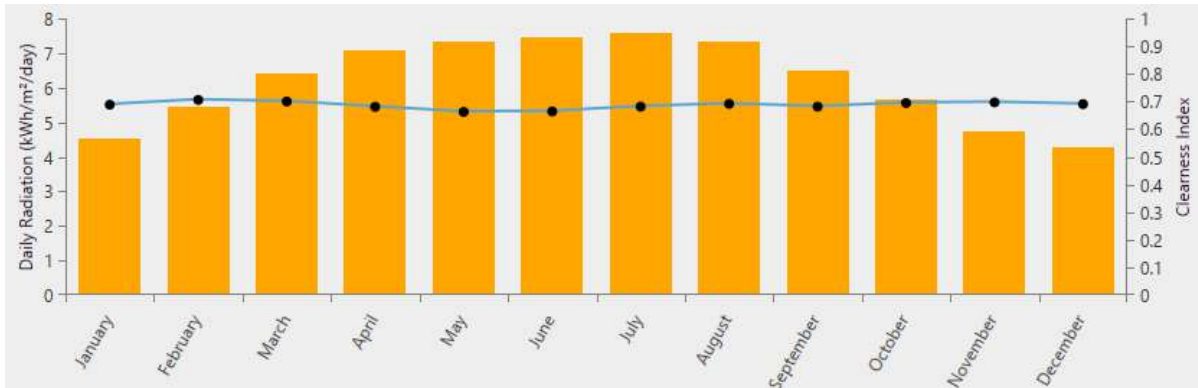


Fig II. 16: Typical yearly profile of the solar radiation

The figure 11 shows the average of global horizontal radiation (orange rectangles) and the cleanness index (blue line) of the studied area (IFNI)

II.3.1.2.1.1.2 Wind resource

Similar to the solar sources resources the software needs the wind speed time series in order to calculate energy produced by the wind turbine

We collected wind speed data from NASA Surface meteorology and Solar Energy database ,where wind speed at 50m above the surface of the earth for terrain similar to airport, monthly averaged values over 10 year period(July1983.June1993) under :

Cell number:115187 Cell demensions:1degree x degree

Cell midpointLatitude: 25.5 Cell midpoint Longitude:7.5

Anemometer height :50 m

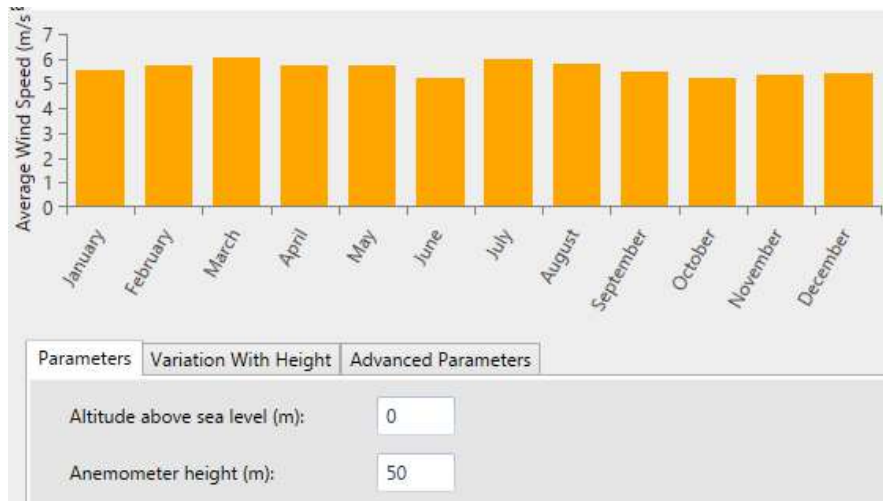


Fig II. 17: monthly average wind speed data

Figure 8 illustrates the monthly average of wind speed data as we can see these speeds are good for a typical wind turbine to generate power the Altitude above sea level is 0m and anemometer height is 50m .

II.3.1.2.1.3 Temperature time series:

The daily average temperature is also needed in some homer calculations

We have collected these a time series data of the daily average temperature of Illizi from 2008 to 2017 from the Algerian national meteorology office in Ourgla ‘regional station’

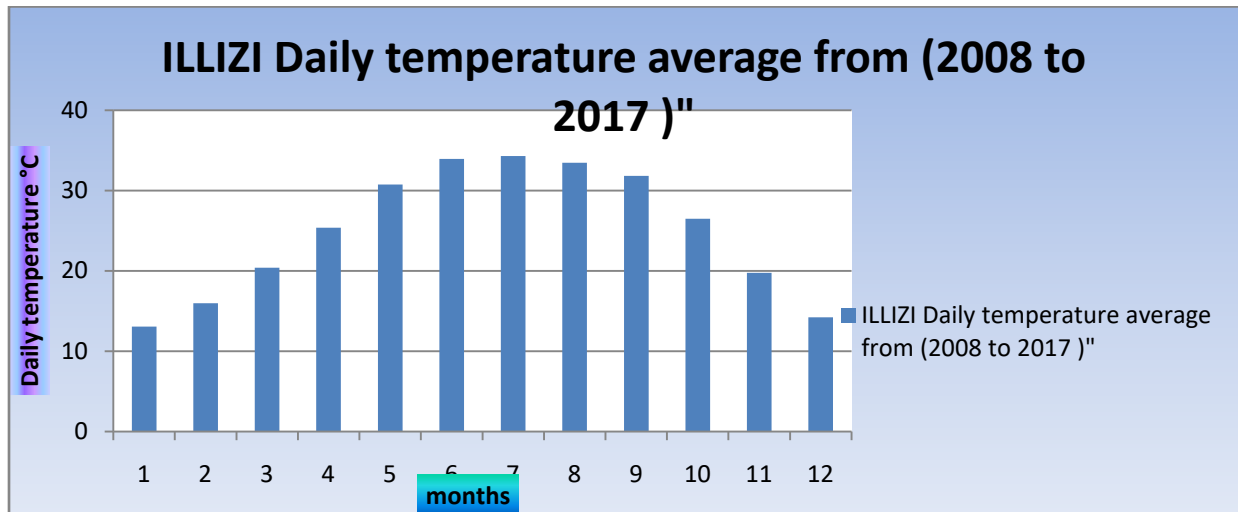


Fig II. 18: daily average temperature (source ‘office national de la meteorologie’ Ourgla- Algeria office)

As we can see from the graph the average temperature increased significantly from May to September

II.3.1.2.2 Load profile:

Since our load is almost constant during all the year except summer period where temperatures raise, we filled the yearly load table so that the energy consumption remains constant except summer month(June, July and August) were the energy increased due to the increasing in air conditioner cooling capacity (for more about dc air conditioner conditions and rated power see appendix B).



Fig II. 19 example of a constant daily load profile

Although the cell site real energy consumption isn't exactly constant during these two periods, so to be more realistic in our load profile we worked in homer random variability two parameters:

Day-to-day: perturb each day's load profile by a random amount, so that the load retains the same shape for each day, but is scaled upwards or downwards[13].

Timestep : the time-step-to-time-step variability disturbs the shape of the load profile without affecting its size[13].

The mechanism for adding day-to-day and time-step-to-time-step variability is simple. First HOMER assembles the year-long array of load data from the daily profiles we specify. Then, it steps through that time series, and in each time step it multiplies the value in that time step by perturbation factor *a* where :

$$a = 1 + \delta_d + \delta_{ts} \quad \text{(II-3)}$$

δ_d = daily perturbation value

δ_{ts} = time step perturbation value

So now after sitting day-today:10.301% and a timestep:19.753%

our load profile became :

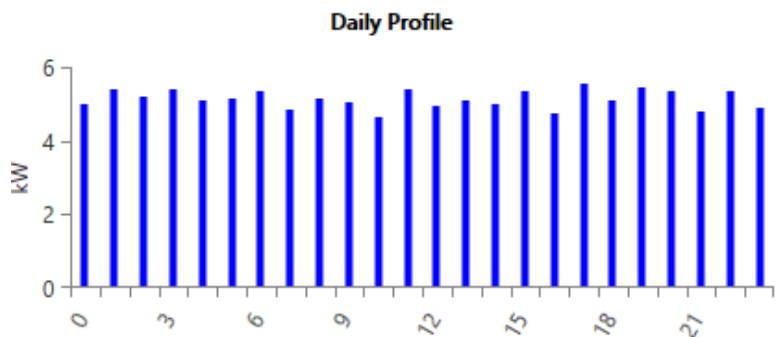


Fig II. 20: Daily load profile of the cell site

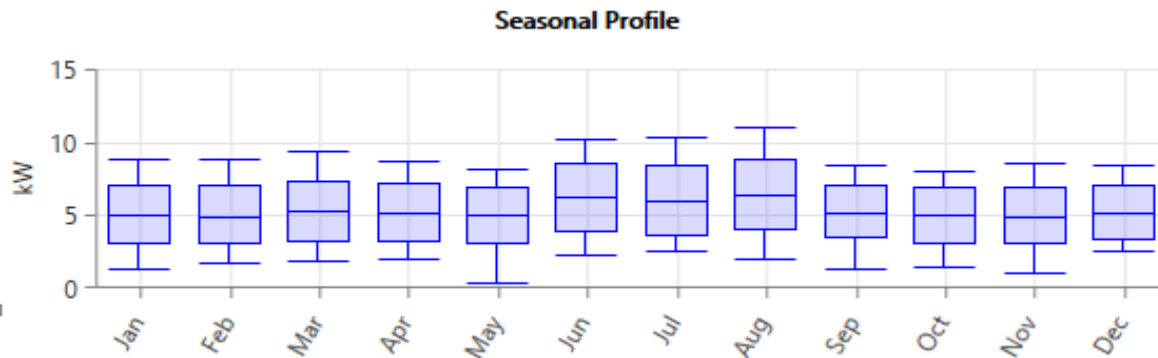


Fig II. 21: Seasonal profile electric load

II.3.1.3 Choose components:

From components ribbon we collected all our desired system components :

PV, Fuel cell generator, Wind turbines , electrolyzer ,Hydrogen Tank

II.3.1.3.1 Components properties:

Each components has each own proprieties

- Variable power sources:

Table II.2 Variable power sources

PV panel	Wind turbine
Name : Generic flat plate PV Abbreviation : PV Panel Type : flat plate Rated capacity (KW): 1 Temperature coefficient: -0.5 Operating Temperature (°C): 47 Efficiency (%): 13 Manufacturer : Generic	Name : Generic 1 KW Abbreviation : G1 Rated capacity (KW): 1 Manufacturer : Generic

- Storage system:

Table II. 3 Storage system

Fuel cell	Electrolyzer	Hydrogen Tank
Name : Fuel cell Abbreviation : FC Manufacturer : Generic	Name : Electrolyzer Abbreviation : Electrolyzer Manufacturer : Generic	Name : Hydrogen Tank Abbreviation : HTank Manufacturer : Generic

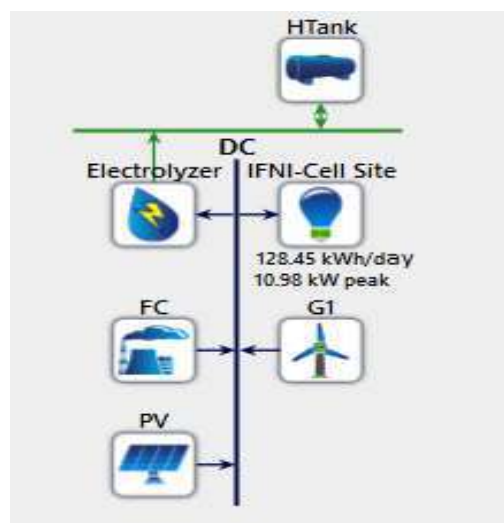


Fig II. 22: Implementation of the stand-alone system

II.3.1.3.2 Components optimization inputs:

II.3.1.3.2.1 Cost Data and Size Specifications of Each Component

Searching the optimum energy system configuration that would meet the demand with minimum NPC and COE. The estimation of the components cost was made based on homer’s given cost for the PV and wind while the storage fuel cell system values used are very rough estimates of 2016 prices.

Some cost definitions:

Initial capital cost of components: The initial capital cost of a component is the total installed cost of that component at the beginning of the project [13].

Operation and Maintenance Cost: The O&M cost of a component is the cost associated with operating and maintaining that component. The total O&M cost of the system is the sum of the O&M costs of each system component. For most components, you enter the O&M cost as an annual amount [13].

Replacement cost: The replacement cost is the cost of replacing a component at the end of its lifetime, as specified by lifetime parameter in the component model [13].

II.3.1.3.2.1.1 Cost optimization inputs:

Table II. 4 components costs

Component Its Cost	PV (1kw)	WTG 1kw	ELECTRO 1kw	FC 1kw	Hydro. Tank 1kg
Capital (\$)	3000	7000	2000	3000	1500
Replacement (\$)	3000	7000	2000	3000	1500
O/M (\$)	10	70	00	0.1	00

II.3.1.3.3 Optimization capacity inputs:

The PV panel’s optimization capacities were left to homer optimizer.

While the other component's capacities are summarized in table below:

Table II. 5 Optimization capacity inputs

Wind1kW turbine gen Quantities	Fuel cell Kw	Electrolyzer Kw	Hydrogen tank Kg
1	10	10	20
2	20	20	40
3	25	30	60
4	50	40	80
5	70	50	100
		60	120
		70	
		80	

Extra Inputs affect the optimization :

PV panels:

We considered the temperature effects on the PV panel where:

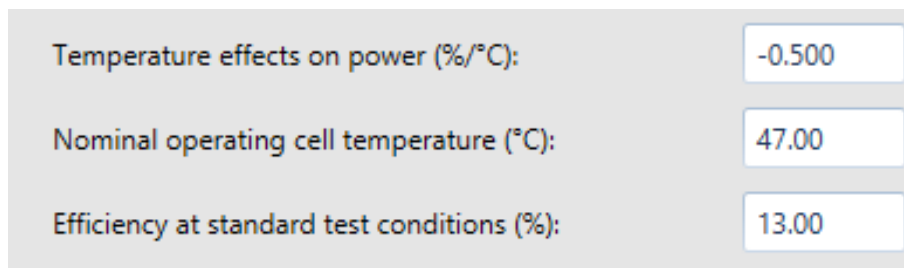


Fig II. 23: temperature effect parameters

- The ground reflectance were 20%
- There is no tracking system considered in this study
- The slop 25.89°
- the azimuth 0° (degrees)

Wind turbine:

- Hub height : 17m

Fuel cell system:

Hydrogen tank :

- Relative initial tank size 10%.
- Require year-end tank level to equal or exceed initial tank level.

Economic inputs:

In our study capacity shortage penalty, system fixed O&M cost, system fixed capital cost was taken as zero, the modeling tool would consider the following additional inputs.

The lifetime of the off-grid power system is designed to end for 25 years long with generating capacity to meet the demand and the nominal rate was taken as 6% with expected inflation rate 2%.

II.3.1.4 Constraints:

Constraints are some energy system desired conditions that should be respected by the system to be feasible. Hence all infeasible systems aren't respect these constraints.

II.3.1.4.1 Maximum annual capacity shortage in %:

It defined as the maximum allowable value of the capacity shortage fraction which is equal to the total capacity shortage divided by the total electrical demand where the total capacity shortage is the total amount of capacity shortage that occurs throughout the year.

In our system we have set the value to be 10%.

II.3.1.4.2 Minimum renewable fraction:

The renewable fraction is the fraction of the energy delivered to the load that originated from renewable power sources. HOMER calculates the renewable fraction using the following equation:

We have set a value of 0% ,since our system is a renewable system this parameters isn't important to check.

II.3.1.5 Sensitivity Variables:

On this study we weren't concerned about sensitivity analysis, so we didn't input sensitivity variables.

II.4 . Chapter summary:

Since we cover on this chapter our project load type and we learn about our design and optimization inputs which based on using homer pro method.

CHAPTER III

CHAPTER III: Power System Modeling

III.1 Introduction:

In order to perform a simulation process to our system we must first model the system including all its components characteristics (power input/output) in form of mathematical equations.

To simplify that model some variables could be neglected, some assumptions could be applied also all input and output in simulation process will take a relative numerical values.

III.2 System modeling:

III.2.1 Solar PV Modeling :

The PV panel often characterizes by two parameters given by the manufacturers:

- a. Open circuit voltage
- b. Short circuit current

I-V curve of the panel is also a main factor to the modeler and it has three main factors to consider,

- a. Short-circuit current,
- b. Open circuit voltage and
- c. Maximum power point.

Equivalent Electrical Circuit of PV Cell

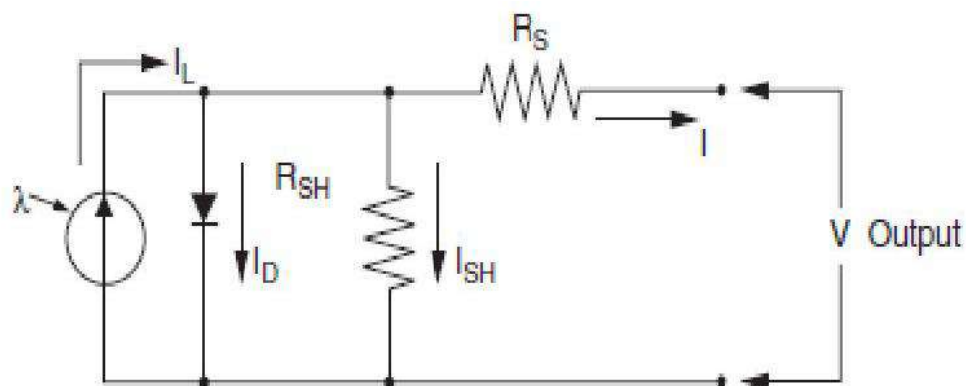


Fig III. 24 Equivalent Circuit of Solar PV Cell [14]

Figure 12 shows as a typical PV cell electrical circuit characteristics.

The different parameters of the photovoltaic cell indicated in the equivalent circuit are expressed by the following mathematical expressions [14].

$$I = I_L - I_D - I_{sh} \quad (\text{III-1})$$

where:

I: PV output current [A]

I_L : solar generated current [A]

I_D : Diode current [A]

I_{sh} : Shunt-leakage current [A]

The yield efficiency of PV panel can be greatly reduced by a small change of the internal resistance developed in the cell however there is no change of output voltage for any change of the shunt resistance [14]. Other mathematical expressions can be applied to determine the output current of the cell as follows.

$$I = I_L - I_o \left[e^{\frac{Q \cdot V_{oc}}{K \cdot T}} - 1 \right] - \frac{V_{oc}}{R_{SH}} \quad (\text{III-2})$$

In actual operating times the last term which represents the shunt current is so small compared to the solar produced and diode currents, thus it can omitted [15] [14]. Temperature variations of the cell are considered uniform in this kind of model [16]. The open circuit voltage and the diode current are being determined as follows respectively:

$$V_{OC} = V + I \cdot R_{SH} \quad (\text{III-3})$$

$$I_D = I_o \left[e^{\frac{Q \cdot V_D}{K \cdot T}} - 1 \right] \quad (\text{III-4})$$

Where:

I_o : Reverses saturation current of diode [A]

Q: Electron charge [C]

K: Boltzmann's constant [J/k]

V_D : Voltage of the diode [V]

T: Cell junction point temperature [k]

V_{OC} : Cell open circuit voltage [V]

Similarly the short circuit current of the cell can be determined by setting the open circuit voltage as zero accordingly the short circuit and solar generated currents remained with the same magnitude. The diode saturation current (I_o) is constant at constant temperature [14] and its mathematical determination is expressed as follows.

$$I_o = \frac{I_{sc}}{e^{Q \cdot V_{oc}} - 1} \quad (III-5)$$

If the short circuit current of the module is known from the data sheet of the cell therefore at any solar irradiance, the cell current is given as follows

$$I_{sc} = \left(\frac{G}{G_o}\right) I_{sc,G_o} \quad (III-6)$$

Where:

I_{sc} : Short circuit current [A]

G: Solar irradiance [W/m^2]

I_{sc,G_o} : Short circuit current at standard test condition [A]

G_o : Solar irradiance at standard test condition [$1000W/m^2$]

The open circuit voltage can be determined by setting the output current to zero.

$$V_{OC} = \frac{AKT}{Q} \log\left(\frac{I_L}{I_o} + 1\right) \quad (III-7)$$

The quality of PV cell is measured by the parameter called fill factor. This shows that an efficient PV will have higher values of short circuit current, open circuit voltage, and filling factor. Any solar PVs fill factor depends on the design and technology of the panel. Whichever parameter or damage that influences the fill factor also disturbs the yield power by reducing

maximum current or maximum voltage or both at the same time. The output power of PV can be calculated using equation 3.23 given in [17].

$$P_{mp} = I_{mp} * V_{mp} \quad (III-8)$$

$$FF = \frac{V_{oc} + I_{sc}}{P_{mp}} \quad (III-9)$$

where:

V_{mp} : PV maximum potential voltage [V]

I_{mp} : PV panels maximum current [A]

P_{mp} : PV panels maximum power [W]

FF : Fill factor

Furthermore, the output power of the PV can also be determined by considering the effect of solar irradiation and environmental temperature at the site of interest. As the expression given in [18] the mathematical expressions for the maximum current and maximum voltage given in equation 3.23 can be determined as follows.

$$V_{mp} = V_{mp.ref} * P_{v,oc} (T_c - T_{c,ref}) \quad (III-10)$$

$$I_{mp} = I_{mp.ref} * I_{sc.ref} (T_c - T_{c,ref}) \quad (III-11)$$

where:

$V_{mp.ref}$: Potential voltage at standard condition [V]

$P_{v,oc}$: Open circuit temperature coefficient [V/k]

$I_{mp.ref}$: PV panels maximum current at standard conditions [A]

$I_{sc.ref}$: PV panels short circuit current at standard condition [A]

T_c : Cell operational temperature [k]

$T_{c,ref}$: Cell temperature at standard conditions [k]

Figure 13 shows a typical PV module I-V characteristic curve

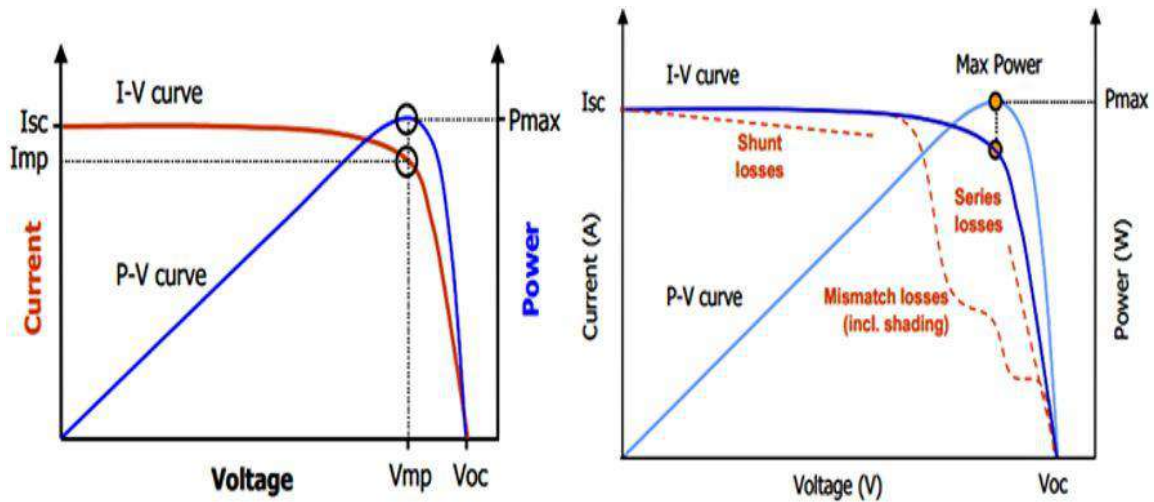


Fig III. 25 Variation of I-V Characteristic Curve of PV Cell with Categories of Different Losses [19]

Referring into figure 13 in the right graph, the series losses & shunt losses, and mismatch losses are resulted due to uniform soiling and non-uniform shadings of the solar PV system respectively.

III.2.1.1 Mathematical modeling:

The mathematical modeling depicts a different approach for the design of a PV array. The performance of solar PV is needed to produce power in an efficient way as much as possible, thus the mathematical model described below is used to determine the optimal power generation characteristics. Having the inputs such as, incident solar radiation data, the local area ambient temperature data, and PV module data supplied by the manufacturers, the PV power output can be determined by the following equations [20] [21].

$$P_{pv} = \eta N A_m G_t \quad (III-12)$$

Where:

P_{pv} : Solar PV power output [W]

η : Generator efficiency [%]

A_m : Area of single module (m^2)

G_t : Global radiation (W/m^2)

N: number of modules assembled in the system

The solar photovoltaic generator efficiency is represented by the following equation.

$$\eta_g = \eta_r \times \eta_{pt} [1 - \beta_t (T_c - T_r)] \quad (III-13)$$

Where:

η_r : Reference efficiency [%]

η_{pt} : tracking system efficiency [%]

T_c : PV cell temperature [k]

T_r : PV cell reference temperature [k]

β_t : Temperature coefficient efficiency ranging from 0.004 to 0.006/°C for silicon cells.

$$T_c = T_a + G_t \left(\frac{\tau\alpha}{UI} \right) \quad (III-14)$$

$$\alpha \cdot \tau / UI = \frac{NOCT-20}{800} \quad (III-15)$$

Where:

T_a : Site ambient temperature [k]

UI: Overall heat loss (W/m²)

τ and α : photovoltaic transmittance and absorptance coefficients respectively .

η_{pt} , β_t , NOCT, A_m : Are parameters that depend on module type and this are obtained from solar module manufacturers.

III.2.1.2 HOMER solar calculations: [13]

III.2.1.2.1 How HOMER Calculates the Radiation Incident on the PV Array:

The Solar GHI resource window allows you to specify the global horizontal radiation (GHI) for each time step in the HOMER simulation. The GHI is the total amount of solar radiation striking the horizontal surface on the earth. But the power output of the PV array depends on the amount of radiation striking the surface of the PV array, which in general is not

horizontal. So in each time step, HOMER must calculate the global solar radiation incident on the surface of the PV array. This article describes that process, which is based on the methods in the first two chapters of Duffie and Beckman (1991)

We can describe the orientation of the PV array using two parameters: a slope, and an azimuth. The slope is the angle formed between the surface of the panel and the horizontal, so a slope of zero indicates a horizontal orientation, whereas a 90° slope indicates a vertical orientation. The azimuth is the direction towards which the surface faces. HOMER uses the convention whereby zero azimuth corresponds to due south, and positive values refer to west-facing orientations. So an azimuth of -45° corresponds to a southeast-facing orientation, and an azimuth of 90° corresponds to a west-facing orientation.

The other factors relevant to the geometry of the situation are the latitude, the time of year, and the time of day. The time of year affects the solar declination, which is the latitude at which the sun's rays are perpendicular to the earth's surface at solar noon. HOMER uses the following equation to calculate the solar declination:

$$\delta = 23.45^\circ \sin\left(360^\circ \frac{284+n}{365}\right) \quad (\text{III-16})$$

where :

n is the day of the year [a number 1 through 365]

The time of day affects the location of the sun in the sky, which we can describe by an hour angle. HOMER uses the convention whereby the hour angle is zero at solar noon (the time of day at which the sun is at its highest point in the sky), negative before solar noon, and positive after solar noon. HOMER uses the following equation to calculate the hour angle:

$$\omega = (t_s - 12hr) * 15^\circ/hr \quad (\text{III-17})$$

where :

t_s is the solar time [hr]

The value of t_s is 12hr at solar noon, and 13.5hr ninety minutes later. The above equation follows from the fact that the sun moves across the sky at 15 degrees per hour.

HOMER assumes that all time-dependent data, such as solar radiation data and electric load data, are specified not in solar time, but in civil time (also called local standard time). HOMER calculates solar time from civil time using the following equation:

$$t_s = t_c + \frac{\lambda}{15^\circ/hr} - Z_c + E \quad (III-18)$$

where :

t_c is the civil time in hours corresponding to the midpoint of the time step [hr]

λ is the longitude [$^\circ$]

Z_c is the time zone in hours east of GMT [hr]

E is the equation of time [hr]

Note that west longitudes are negative, and time zones west of GMT are negative as well.

The equation of time accounts for the effects of obliquity (the tilt of the earth's axis of rotation relative to the plane of the ecliptic) and the eccentricity of the earth's orbit. HOMER calculates the equation of time as follows:

$$E = 3.82 \left(\begin{array}{l} 0.000075 + 0.001868 * \cos B - 0.032077 * \sin B \\ - 0.014615 * \cos 2B - 0.04089 * \sin 2B \end{array} \right) \quad (III-19)$$

where B is given by:

$$B = 360^\circ \frac{(n-1)}{365} \quad (III-20)$$

where n is the day of the year, starting with 1 for January 1st.

Now, for a surface with any orientation, we can define the angle of incidence, meaning the angle between the sun's beam radiation and the normal to the surface, using the following equation:

$$\begin{aligned} \cos\theta = \sin\delta \sin\phi \cos\beta - \sin\delta \cos\phi \sin\beta \cos\gamma + \cos\delta \cos\phi \cos\beta \cos\omega \\ + \cos\delta \sin\phi \sin\beta \cos\gamma \cos\omega + \cos\delta \sin\beta \sin\gamma \sin\omega \end{aligned} \quad (III-21)$$

where :

θ is the angle of incidence [$^\circ$]

β is the slope of the surface [$^{\circ}$]

γ is the azimuth of the surface [$^{\circ}$]

ϕ is the latitude [$^{\circ}$]

δ is the solar declination [$^{\circ}$]

ω is the hour angle [$^{\circ}$]

An incidence angle of particular importance, which we will need shortly, is the zenith angle, meaning the angle between a vertical line and the line to the sun. The zenith angle is zero when the sun is directly overhead and 90° when the sun is at the horizon. Because a horizontal surface has a slope of zero, we can find an equation for the zenith angle by setting $\beta = 0^{\circ}$ in the above equation, which yields:

$$\cos\theta_z = \cos\phi \cos\delta \cos\omega + \sin\phi \sin\delta \quad (\text{III-22})$$

where :

θ_z is the zenith angle [$^{\circ}$]

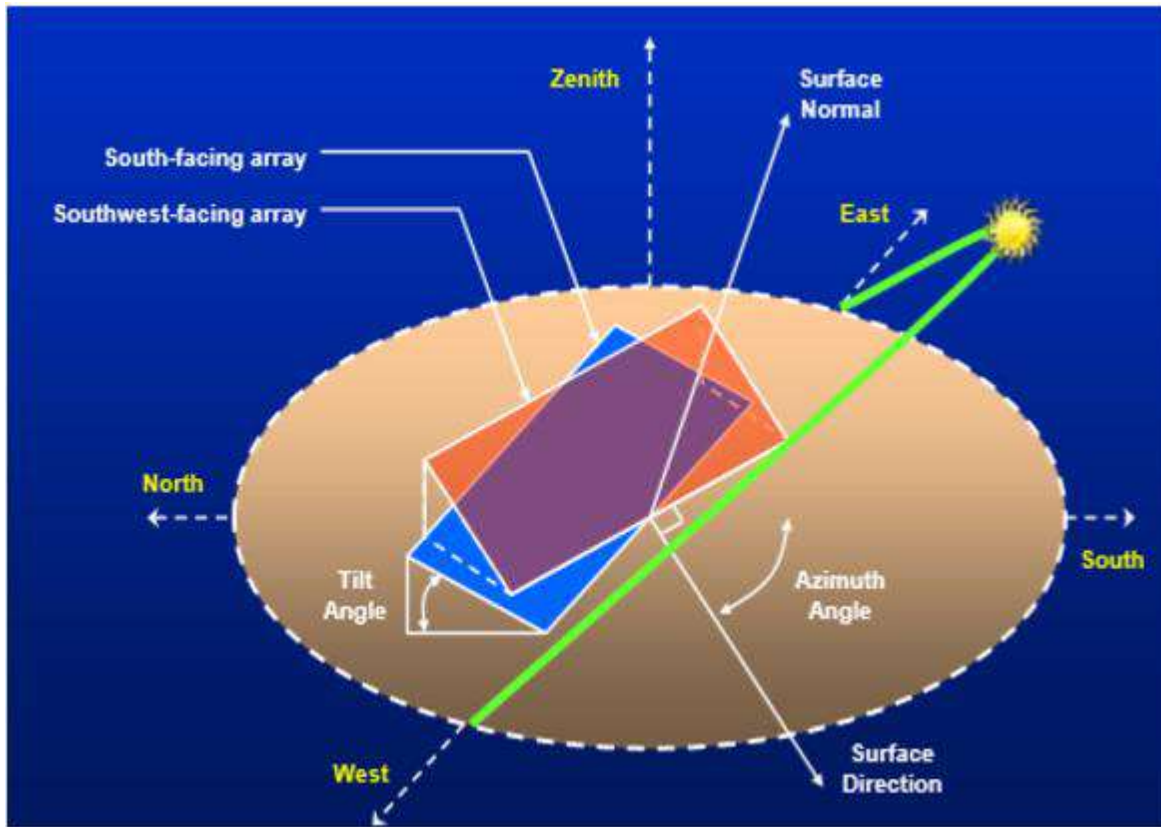


Fig III .26 Orientation and Slope of Solar PV Module [22]

Now we turn to the issue of the amount of solar radiation arriving at the top of the atmosphere over a particular point on the earth's surface. HOMER assumes the output of the sun is constant in time. But the amount of sunlight striking the top of the earth's atmosphere varies over the year because the distance between the sun and the earth varies over the year due to the eccentricity of earth's orbit. To calculate the extraterrestrial normal radiation, defined as the amount of solar radiation striking a surface normal (perpendicular) to the sun's rays at the top of the earth's atmosphere, HOMER uses the following equation:

$$G_{on} = G_{sc} \left(1 + 0.033 * \cos \frac{360n}{365} \right) \quad \text{(III-23)}$$

where :

G_{on} is the extraterrestrial normal radiation [kW/m²]

G_{sc} is the solar constant [1.367 kW/m²]

n is the day of the year [a number between 1 and 365]

To calculate the extraterrestrial horizontal radiation, defined as the amount of solar radiation striking a horizontal surface at the top of the atmosphere, HOMER uses the following equation:

$$G_o = G_{on} \cos\theta_z \quad (\text{III-24})$$

where :

G_o is the extraterrestrial horizontal radiation [kW/m²]

G_{on} is the extraterrestrial normal radiation [kW/m²]

θ_z is the zenith angle [°]

Since HOMER simulates on a time step by time step basis, we integrate the above equation over one time step to find the average extraterrestrial horizontal radiation over the time step:

$$\bar{G}_o = \frac{12}{\pi} G_{on} \left[\cos\phi \cos\delta (\sin\omega_2 - \sin\omega_1) + \frac{\pi(\omega_2 - \omega_1)}{180^\circ} \sin\phi \sin\delta \right] \quad (\text{III-25})$$

where :

\bar{G}_{on} is the extraterrestrial horizontal radiation averaged over the time step [kW/m²]

G_{on} is the extraterrestrial normal radiation [kW/m²]

ω_1 is the hour angle at the beginning of the time step [°]

ω_2 is the hour angle at the end of the time step [°]

The above equation gives the average amount of solar radiation striking a horizontal surface at the top of the atmosphere in any time step. The solar resource data give the average amount of solar radiation striking a horizontal surface at the bottom of the atmosphere (the surface of the earth) in every time step. The ratio of the surface radiation to the extraterrestrial radiation is called the clearness index. The following equation defines the clearness index:

$$k_T = \frac{\bar{G}}{\bar{G}_o} \quad (\text{III-26})$$

where :

\bar{G} is the global horizontal radiation on the earth's surface averaged over the time step [kW/m²]

\bar{G}_0 is the extraterrestrial horizontal radiation averaged over the time step [kW/m²]

Now let us look more closely at the solar radiation on the earth's surface. Some of that radiation is beam radiation, defined as solar radiation that travels from the sun to the earth's surface without any scattering by the atmosphere. Beam radiation (sometimes called direct radiation) casts a shadow. The rest of the radiation is diffuse radiation, defined as solar radiation whose direction has been changed by the earth's atmosphere. Diffuse radiation comes from all parts of the sky and does not cast a shadow. The sum of beam and diffuse radiation is called global solar radiation, a relation expressed by the following equation:

$$\bar{G}_0 = \bar{G}_b + \bar{G}_d \quad (\text{III-27})$$

where :

\bar{G}_b is the beam radiation [kW/m²]

\bar{G}_d is the diffuse radiation [kW/m²]

The distinction between beam and diffuse radiation is important when calculating the amount of radiation incident on an inclined surface. The orientation of the surface has a stronger effect on the beam radiation, which comes from only one part of the sky, than it does on the diffuse radiation, which comes from all parts of the sky.

However, in most cases we measure only the global horizontal radiation, not its beam and diffuse components. For that reason, HOMER expects you to enter global horizontal radiation in HOMER's Solar Resource Inputs window. That means that in every time step, HOMER must resolve the global horizontal radiation into its beam and diffuse components to find the radiation incident on the PV array. For this purpose HOMER uses correlation of Erbs et al. (1982), which gives the diffuse fraction as a function of the clearness index as follows:

$$\frac{\bar{G}_d}{\bar{G}} = \begin{cases} 1.0 - 0.09k_T & \text{for } k_T \leq 0.22 \\ 0.9511 - 0.1604k_T + 4.388k_T^2 - 16.638k_T^3 + 12.336k_T^4 & \text{for } 0.22 \leq k_T \leq 0.80 \\ 0.165 & \text{for } k_T > 0.80 \end{cases}$$

$$(\text{III-28})$$

For each time step, HOMER uses the average global horizontal radiation to calculate the clearness index, then the diffuse radiation. It then calculates the beam radiation by subtracting the diffuse radiation from the global horizontal radiation.

HOMER software uses the following equation to calculate the output of the PV array:

$$P_{PV} = Y_{PV} f_{PV} \left(\frac{\bar{G}_T}{\bar{G}_{T,STC}} \right) [1 + \alpha_P (T_c - T_{c,STC})] \quad (III-29)$$

where :

Y_{PV} is the rated capacity of the PV array, meaning its power output under standard test conditions [kW]

f_{PV} is the PV derating factor [%]

\bar{G}_T is the solar radiation incident on the PV array in the current time step [kW/m²]

$\bar{G}_{T,STC}$ is the incident radiation at standard test conditions [1 kW/m²]

α_P is the temperature coefficient of power [%/°C]

T_c is the PV cell temperature in the current time step [°C]

$T_{c,STC}$ is the PV cell temperature under standard test conditions [25 °C]

III.2.1.2.2 How HOMER Calculates Clearness Index:

On the Solar Resource window, for each month of the year you can enter the average radiation for the month. Based on the value of the average radiation, the month of the year, and the latitude, HOMER calculates the clearness index. This article describes the relationship between the two variables, and how HOMER calculates clearness index from the global horizontal radiation (GHI).

The clearness index is a dimensionless number between 0 and 1 indicating the fraction of the solar radiation striking the top of the atmosphere that makes it through the atmosphere to strike the Earth's surface. The following equation defines the monthly average clearness index:

$$K_T = \frac{H_{ave}}{H_{o,ave}} \quad (III-30)$$

where :

H_{ave} is the monthly average radiation on the horizontal surface of the earth [kWh/m²/day]

$H_{o,ave}$ is the extraterrestrial horizontal radiation, meaning the radiation on a horizontal surface at the top of the earth's atmosphere [kWh/m² /day]

For a given latitude, we can calculate $H_{o,ave}$ for any month of the year. So if we know either H_{ave} or K_T , we can calculate the other using the above equation. HOMER does exactly that every time you enter a value into the monthly data table on the Solar Resource Inputs window. If you enter an average radiation value, HOMER will calculate the corresponding clearness index.

The rest of this article describes how HOMER calculates $H_{o,ave}$, the monthly average extraterrestrial radiation.

As described in more detail in the article on calculating the radiation incident on the PV array, HOMER uses the following equation to calculate the intensity of solar radiation at the top of the Earth's atmosphere:

$$G_{on} = G_{sc} \left(1 + 0.033 * \cos \frac{360n}{365} \right) \quad \text{(III-31)}$$

where :

G_{sc} is the solar constant [1.367 kW/m²]

n is the day of the year [a number between 1 and 365]

The equation above gives the extraterrestrial radiation on a surface normal to the sun's rays. To calculate the extraterrestrial radiation on the horizontal surface, HOMER uses the following equation:

$$G_o = G_{on} \cos \theta_Z \quad \text{(III-32)}$$

where :

θ_Z is the zenith angle [°]

HOMER calculates the zenith angle using the following equation:

$$\cos \theta_Z = \cos \phi \cos \delta \cos \omega + \sin \phi \sin \delta$$

where :

ϕ is the latitude [$^{\circ}$]

δ is the solar declination [$^{\circ}$]

ω is the hour angle [$^{\circ}$]

HOMER calculates the solar declination according to the following equation:

$$\delta = 23.45^{\circ} \sin \left(360^{\circ} * \frac{284+n}{365} \right) \quad (\text{III-33})$$

where :

n is the day of the year [a number between 1 and 365]

We can find the total daily extraterrestrial radiation per square meter by integrating the equation for G_o from sunrise to sunset. This integration gives the following equation:

$$H_o = \frac{24}{\pi} G_{on} \left[\cos\phi \cos\delta \sin\omega_s + \frac{\pi\omega_s}{180^{\circ}} \sin\phi \sin\delta \right]$$

where :

H_o is the average extraterrestrial horizontal radiation for the day [kWh/m²/day]

ω_s is the sunset hour angle [$^{\circ}$]

HOMER calculates the sunset hour angle using the following equation:

$$\cos\omega_s = -\tan\phi \tan\delta \quad (\text{III-34})$$

HOMER calculates H_o for each day of the month, and finds the average for the month as follows:

$$H_{o,ave} = \frac{\sum_{n=1}^N H_o}{N} \quad (\text{III-35})$$

where :

$H_{o,ave}$ is the average extraterrestrial horizontal radiation for the month [kWh/m²/day]

N is the number of days in the month

If you enter the monthly average global solar radiation, HOMER divides it by $H_{o,ave}$ to find the monthly average clearness index.

III.2.2 Wind turbine modeling:

III.2.2.1 Power output:

Electrical power of the wind turbine is expressed mathematically as [23].

$$P_{el} = \frac{1}{2} \rho A V^3 C_p \eta_g \eta_m \quad (\text{III-36})$$

Where:

P_{el} : wind turbine electrical power [kW]

η_m : The mechanical (gear box) [%]

η_g : Electrical generator efficiencies [%]

$$C_p = \frac{\text{maximum power extracted}}{\text{power availabl in the wind}} = \frac{\rho A V_1^3 \left(\frac{8}{27}\right)}{\frac{1}{2} \rho A V_1^3} = \frac{16}{27} \quad (\text{III-37})$$

where:

C_p : Performance coefficient or wind flow condition

The rotor efficiency has a theoretical maximum value of 0.593, and it is called the Betz limit.

In real cases due to lose the maximum value of C_p is 0.4 and 0.5 for two blade rotor and between 0.2 and 0.4 for more blade as well as low speed turbines (24).

In our study we considered a three blade horizontal wind turbine due to its popularity.

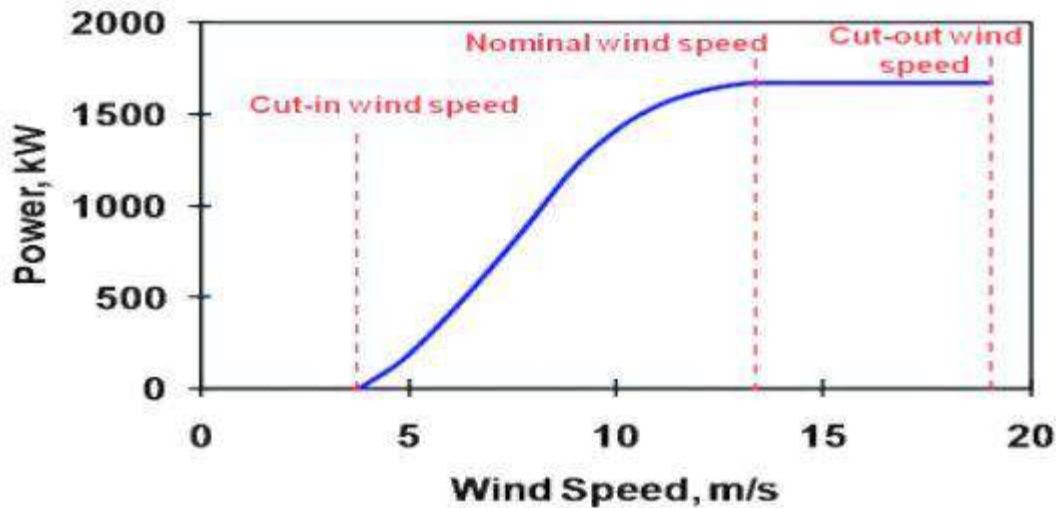


Fig III. 27 Characteristic Curve of Typical Wind Turbine [24]

Figure 14 is the general characteristic curve of a wind turbine, which exhibits wind turbine power output variation with wind speed. In the characteristics curve of any wind turbine there are

The figure 14 shows a general characteristic of any wind turbine as we see can from the curve there are three main value of wind speed .

a. Cut-in Wind Speed:

The speed at which the wind turbine starts to generate power from the figure curve above its nearly 5m/s.

b. Cut-off Wind Speed:

It is the highest wind speed at which wind turbines not being produced power rather should stop to protect from damage. For most turbines the cut off speed is 25 m/s [25].

c. Rated Wind Speed:

The wind speed at which the maximum power is derived. This wind speed is the most important one which determines the power curve. Beyond this wind speed higher power generation is possible with special control to the power output to reduce rotor blade stress. Power curves having lower rated speed produce more energy because it will produce more energy

between cut-in and rated wind speed. For most turbines the rated wind speed is between 11.5 to 15 m/sec [26] [25].

d. Survival Speed:

Any wind turbine machine will not able to with stand wind speed beyond the cut out wind speed. It is not actually part of the power curve, but important to specify the design wind speed of the turbine. The range of survival speed is between 50 to 60 m/sec [25].

III.2.2.2 HOMER wind calculations (13):

III.2.2.2.1 How HOMER Calculates Wind Turbine Power Output:

HOMER calculates the power output of the wind turbine in each time step. This entails a three-step process to first calculate the wind speed at the hub height of the wind turbine, then to calculate how much power the wind turbine would produce at that wind speed at standard air density, then to adjust that power output value for the actual air density.

Calculating Hub Height Wind Speed

In each time step, HOMER calculates the wind speed at the hub height of the wind turbine using the inputs you specify in the Wind Resource window and the Wind Shear window.

If you choose to apply the logarithmic law, HOMER calculates the hub height wind speed using the following equation:

$$U_{hub} = U_{anem} * \frac{\ln(z_{hub} / z_0)}{\ln(z_{anem} / z_0)} \quad (III-38)$$

where :

U_{hub} = the wind speed at the hub height of the wind turbine [m/s]

U_{anem} = the wind speed at anemometer height [m/s]

z_{hub} = the hub height of the wind turbine [m]

z_{anem} = the anemometer height [m]

z_0 = the surface roughness length [m]

$\ln(..)$ = the natural logarithm

If you choose to apply the power law, HOMER calculates the hub height wind speed using the following equation:

$$U_{hub} = U_{anem} * \left(\frac{z_{hub}}{z_{anem}} \right)^\alpha \quad (\text{III-39})$$

where :

U_{hub} = the wind speed at the hub height of the wind turbine [m/s]

U_{anem} = the wind speed at anemometer height [m/s]

z_{hub} = the hub height of the wind turbine [m]

z_{anem} = the anemometer height [m]

α = the power law exponent

III.2.2.2.2 Calculating Turbine Power Output At Standard Air Density

Once HOMER has determined the hub height wind speed, it refers to the wind turbine's power curve to calculate the power output one would expect from that wind turbine at that wind speed under standard conditions of temperature and pressure. In the diagram below, the red dotted line indicates the hub height wind speed, and the blue dotted line indicates the wind turbine power output that the power curve predicts for that wind speed.

If the wind speed at the turbine hub height is not within the range defined in the power curve, the turbine will produce no power. This follows the assumption that wind turbines produce no power at wind speeds below the minimum cutoff or above the maximum cut-out wind speeds.

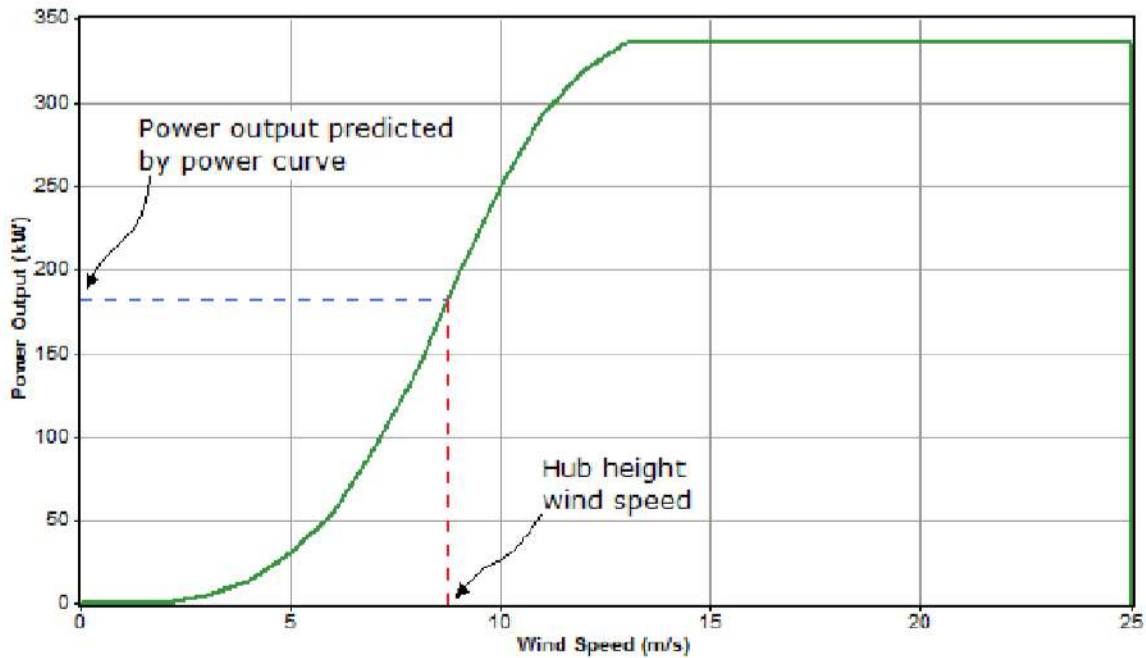


Fig III. 28 HOMER example of wind turbine power*wind speed curve [13]

III.2.2.3

III.2.2.3.1 Applying Density Correction

Power curves typically specify wind turbine performance under conditions of standard temperature and pressure (STP). To adjust to actual conditions, HOMER multiplies the power value predicted by the power curve by the air density ratio, according to following equation:

$$P_{WTG} = \left(\frac{\rho}{\rho_0}\right) * P_{WTG,STP} \quad (III-42)$$

where :

P_{WTG} = the wind turbine power output [kW]

$P_{WTG,STP}$ = the wind turbine power output at standard temperature and pressure [kW]

ρ = the actual air density [kg/m³]

ρ_0 = the air density at standard temperature and pressure (1.225 kg/m³)

III.2.3 PEM fuel cell modeling:

Fuel cells basically convert chemical energy of hydrocarbon fuels directly into dc form of electrical energy. A FCPP mainly consists of a fuel-processing unit (reformer), fuel cell stack

and power-conditioning unit. The fuel cell uses hydrogen as input and produces dc power at the output of the stack. The performance of a fuel cell is generally characterized by using the polarization curve, which is a plot of the fuel cell output voltage as a function of load current. The polarization curve is computed by using the Tafel equation , which subtracts the various voltage losses from the open circuit dc voltage, and is expressed as

$$V_{stack} = V_{open} - V_{ohmic} - V_{activation} - V_{ohmic} - V_{concentration} \quad (III-40)$$

Where:

$$V_{open} = N_0(E^0 + E^1) = N_0 \left[-\frac{\Delta \bar{g}_f^0}{2F} + \frac{RT}{2F} \ln \left(\frac{p_{H_2} \sqrt{p_{O_2}}}{p_{H_2O}} \right) \right] \quad (III-41)$$

$$V_{ohmic} = (i + i_n)R_{FC} = I_{dc} R_{FC} \quad (III-42)$$

$$V_{activation} = N_0 \frac{RT}{2\alpha F} \ln \left(\frac{I_{dc}}{I_0} \right) \quad (III-43)$$

$$V_{concentration} = -c \ln \left(1 - \frac{I_{dc}}{I_{Lim}} \right) \quad (III-44)$$

In the above equations, N_0 is the cell number, V_{open} is the open cell voltage, R is the universal gas constant, T is the temperature of the fuel cell stack, F is the Faraday's constant, p_{H_2} is the hydrogen partial pressure, p_{H_2O} is the water partial pressure, p_{O_2} is the oxygen partial pressure, pO is the standard pressure, α represents the charge transfer coefficient of the electrodes, I_{dc} is the current of the fuel cell stack, I_{Lim} is the limiting current of fuel cell stack, I_0 is the exchange current of fuel cell stack and c is the empirical coefficient for concentration voltage. (all FC equations are on the appendix A) [27]

For a PEM fuel cell system, the exergetic efficiency is defined as

$$\varepsilon = \frac{\text{electrical output}}{(\text{exergy})_{Rxtnt} - (\text{exergy})_{Prdct}} \quad (III-45)$$

$$\varepsilon = \frac{\hat{W}_{net}}{(\hat{E}_{O_2,R} + \hat{E}_{H_2,R}) - (\hat{E}_{O_2,P} + \hat{E}_{H_2O,P})} \quad (III-46)$$

Where $\hat{E}_{O_2,R}$, $\hat{E}_{H_2,R}$, $\hat{E}_{O_2,P}$, and $\hat{E}_{H_2O,P}$ are the total exergies of the reactants, oxygen, and fuel (hydrogen), and the products oxygen and water, respectively. The net electrical power output produced by the cell is given as (III-40)

$$\widehat{W}_{net} = V_{cell} * I \quad (\text{III-47})$$

where V_{cell} is the fuel cell output voltage and I is the current.

The computer simulation of the model developed for theoretical energy and energy analyses of the proton exchange membrane fuel cell is achieved using computer codes to demonstrate the performance and behavior of the system by varying the operating parameters [27].

III.3 Chapter summary:

We learned from this chapter the mathematical model of our hybrid renewable system, we also discovered how homer software uses some methods to calculate the output of the energy sources and how it deal with input.

CHAPTER IV

CHAPTER IV: Results and Discussion

IV.1 Introduction:

On this chapter would give the details of the optimization results for the selected hybrid power system of a typical cell site. The system was designed with the help of HOMER with no given much concern to the load variability and expansion.

As HOMER pro simulated various configurations of our energy system components, but it only displays the feasible power schemes scenarios. The complexity and computation time are affected by the number of parameters(components, sensitivity analysis inputs,...) , total number of potential values involved in the design and also the time step.

By giving all of the input variables in to the modeling tool and check the calculate prompt HOMER runs repeatedly to get solutions.

IV.2 System optimization and simulation

Using a 64-bit operating system, INTEL i5 x64-based 2.6 GHz processor and 6 G.B of RAM on a laptop computer, homer's calculations were done and the calculation report were as follows :

- 25682 solutions were simulated
- 13912 of them was feasible
- 7680 were infeasible due to capacity shortage constraint
- 11770 were infeasible due to hydrogen tank level
- 3840 where omitted due to infeasibility

For each sensitivity case that it solves, HOMER simulates every system in the Search Space and shows all the feasible systems which meets the load and the inputs constraints made by the modeler

Optimization results are displayed from up to down in the form of overall where all feasible system displayed based on their NPC(Net Present Cost) , and categorized where only the least cost effective combinations from among all components setup displayed .

On top of these parameters less cost of energy, high renewable fraction, low capacity shortage and low excess electricity generation could be used for comparison of power generating schemes in order to check their technical feasibility

Since we forced the system to use wind power and only one storage system we only get one power scenario (**pv,wind,fuel cell**)

The optimum system from that scenario showed up in categorized view with that less NPC(net present cost), less COE(cost of energy), higher renewable fraction, lowest capacity shortage, smaller excess electricity .

the figure1 shows this system

Architecture								Cost				System	
PV (kW)	G1	FC (kW)	Electrolyze (kW)	HTank (kg)	Dispi	COE (\$)	NPC (\$)	Operating cost (\$/yr)	Initial capital (\$)	Ren Frac (%)	Total Fuel (L/yr)		
48.8	1	10.0	30.0	20.0	LF	\$0.596	\$419,424	\$9,279	\$273,250	100	1,360		

Fig IV. 29 optimum proposed system(categorized mode)

As we see can from these figure HOMER shows only the best system from that scenario .

NOTE: "Ren. Frac." is an abbreviation of the renewable fraction (for further information about it see chapter 2)

Architecture									Cost				System	
PV (kW)	G1	FC (kW)	Electrolyze (kW)	HTank (kg)	Dispa	COE (\$)	NPC (\$)	Operating cost (\$/yr)	Initial capital (\$)	Ren Frac (%)	Total Fuel (L/yr)			
48.8	1	10.0	30.0	20.0	CC	\$0.596	\$419,424	\$9,279	\$273,250	100	1,360			
48.8	1	10.0	30.0	20.0	LF	\$0.596	\$419,424	\$9,279	\$273,250	100	1,360			
49.2	1	10.0	30.0	20.0	CC	\$0.597	\$421,431	\$9,328	\$274,500	100	1,369			
49.2	1	10.0	30.0	20.0	LF	\$0.597	\$421,431	\$9,328	\$274,500	100	1,369			
49.6	1	10.0	30.0	20.0	CC	\$0.597	\$423,411	\$9,374	\$275,750	100	1,378			
49.6	1	10.0	30.0	20.0	LF	\$0.597	\$423,411	\$9,374	\$275,750	100	1,378			
50.0	1	10.0	30.0	20.0	CC	\$0.598	\$425,231	\$9,410	\$277,000	100	1,386			
50.0	1	10.0	30.0	20.0	LF	\$0.598	\$425,231	\$9,410	\$277,000	100	1,386			
48.3	2	10.0	30.0	20.0	CC	\$0.605	\$428,564	\$9,495	\$279,000	100	1,352			
48.3	2	10.0	30.0	20.0	LF	\$0.605	\$428,564	\$9,495	\$279,000	100	1,352			
48.8	2	10.0	30.0	20.0	CC	\$0.606	\$430,464	\$9,536	\$280,250	100	1,361			
48.8	2	10.0	30.0	20.0	LF	\$0.606	\$430,464	\$9,536	\$280,250	100	1,361			
51.7	1	10.0	30.0	20.0	CC	\$0.602	\$431,633	\$9,499	\$282,000	100	1,407			
51.7	1	10.0	30.0	20.0	LF	\$0.602	\$431,633	\$9,499	\$282,000	100	1,407			
49.2	2	10.0	30.0	20.0	CC	\$0.607	\$432,337	\$9,575	\$281,500	100	1,368			
49.2	2	10.0	30.0	20.0	LF	\$0.607	\$432,337	\$9,575	\$281,500	100	1,368			

Fig IV. 30 system ranked in tabular mode

As we see can from This figure HOMER computes that efficient system in such a way that the lowest NPC ranked or listed in row 1 of the simulation

NOTE: if two system didn't much only in the dispatch strategy, CC dispatch strategy is always ranked by HOMER before LF dispatch strategy.

IV.2.1 Optimum Systems descriptions:

IV.2.1.1 Schematic:

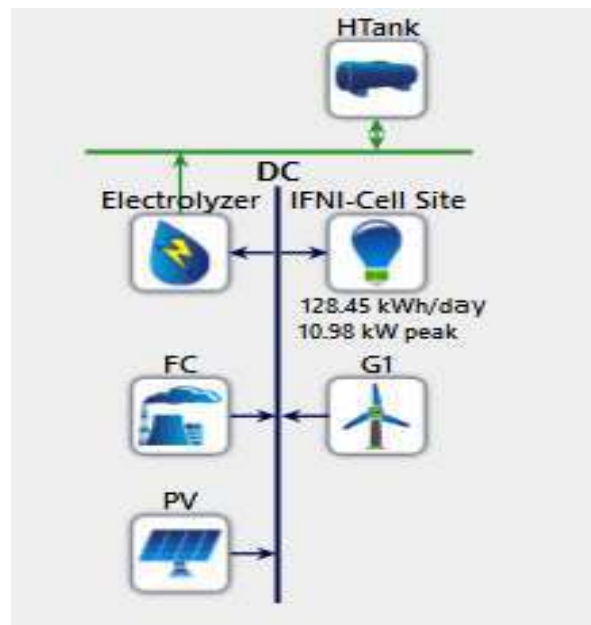


Fig IV. 31 system schematic

This figure show the synoptic scheme of our hybrid power system wich consist of the wind , PV sources and the fuel cell storage system (Fuel cell generator, electrolyzer and a hydrogen tank) plus the load

IV.2.2 System Architecture

Table IV. 1 system architecture

Component	Name	Size	Unit
Generator	Fuel Cell	10.0	kW
PV	Generic flat plate PV	48.8	kW
Wind turbine	Generic 1 kW	1	ea.
Electrolyzer	Electrolyzer	30.0	kW
Hydrogen tank	Hydrogen Tank	20.0	kg
Dispatch strategy	HOMER Load Following		

The previous table shows the system architecture, where

- the fuel cell generator was sized to be 10kW, electrolyzer of 30kW and a hydrogen tank of 20 kg.
- PV array of 48.8kW (49 panels) and that's seems reasonable because of the location height solar irradiation ,
- wind turbine of 1 kW(only one generator) that's make sense because when we saw the wind generator power x speed curve we noticed that the rated wind generator rated speed was far from the location average wind speed .
- The chosen dispatch strategy was HOMER Load following

IV.2.2.1 Load following dispatch strategy description:

The load following strategy is a dispatch strategy whereby whenever a generator operates (which is the fuel cell in our case), it produces only enough power to meet the primary load(cell site). Lower-priority objective such as charging the storage bank (electrolyzer + hydrogen tank) is left to the renewable power sources (wind and PV).

Under the load following strategy, HOMER dispatches the system's controllable power sources (fuel cell generator) so as to serve the primary load(cell site) at the least total cost each time step, while satisfying the operating reserve requirement.

The total cost includes the cost of fuel, operation and maintenance, and replacement.

To accomplish this, HOMER calculates the fixed and marginal cost of the fuel cell generator

Where: its fixed cost is equal to its hourly operation and maintenance cost plus its hourly replacement cost plus the cost of its no-load fuel consumption. Its marginal cost is equal to its fuel curve slope times the fuel price.

The storage bank's (hydrogen tank) fixed cost is zero and its marginal cost is equal to the storage wear cost which is the cost of cycling energy through the storage bank. HOMER assumes the storage bank (hydrogen tank) will require replacement once its total throughput equals its lifetime throughput.

Each kWh of throughput therefore brings the storage bank that much closer to needing replacement. HOMER calculates the storage wear cost using the following equation

$$C_{bw} = \frac{C_{rep.batt}}{N_{bat} \cdot Q_{lifetime} \cdot \sqrt{n_{rt}}}$$

$C_{rep.batt}$: Replacement cost of the storage bank [\$]

N_{bat} : The number of batteries in the storage bank

$Q_{lifetime}$: The lifetime throughput of a single storage [kWh]

n_{rt} : Storage roundtrip efficiency [fractional]

Where the storage bank in our system is the hydrogen tank

Once it characterizes the fuel cell generator in this way, HOMER searches for the combination of generation way that satisfies the primary load, required and operating reserve at least cost.

IV.2.3 System power sources:

IV.2.3.1 Generator: Fuel Cell (Stored hydrogen)

IV.2.3.1.1 Fuel Cell Summary:

Table IV. 2 Fuel Cell Summary

Quantity	Value	Units
Electrical Production	22,659	kWh/yr
Mean Electrical Output	4.84	kW
Minimum Electrical Output	0.0204	kW
Maximum Electrical Output	9.87	kW
Specific Fuel Consumption	0.0600	kg/kWh
Fuel Energy Input	45,319	kWh/yr
Mean Electrical Efficiency	50.0	%

Noticed that the mean fuel cell efficiency is acceptable

IV.2.3.1.2 Fuel Cell Statistics:

Table IV. 1 Fuel Cell Statistics

Quantity	Value	Units
Hours of Operation	4,684	hrs/yr
Number of Starts	380	starts/yr
Operational Life	8.54	Yr
Capacity Factor	25.9	%
Fixed Generation Cost	1.75	\$/hr
Marginal Generation Cost	0	\$/kWh

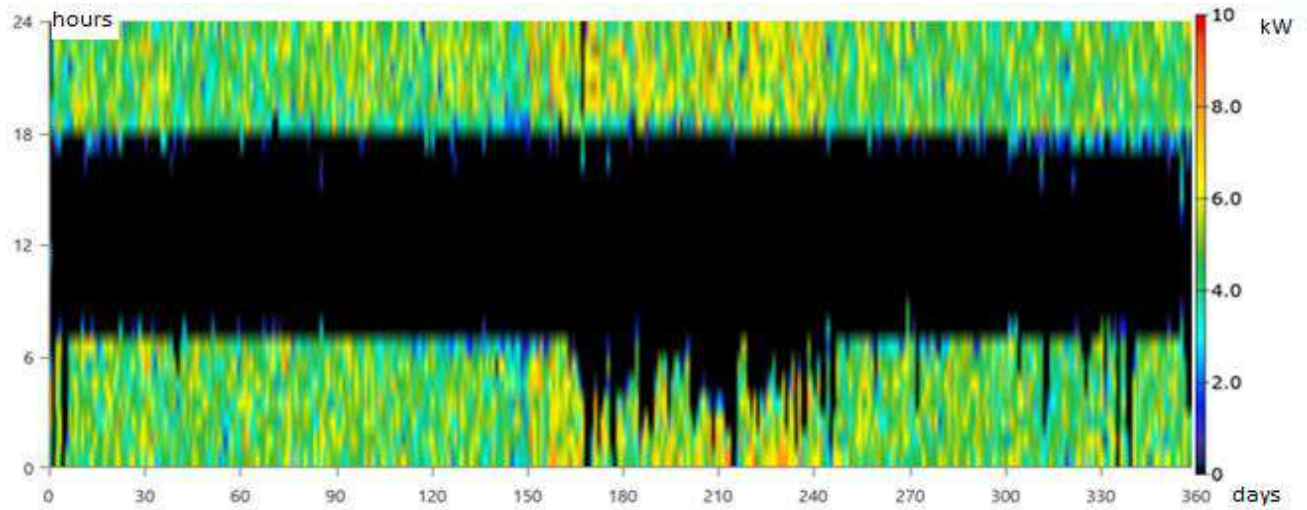


Fig IV. 32 Fuel cell gen Dmap

Noticed that the fuel cell generator provide almost the same amount of power during the year at low solar irradiation time except during summer time where its given amount of power

changed and its working time changes as well due to the effect of solar declination in summer in our location .

IV.2.3.2 PV: Generic flat plate PV

IV.2.3.2.1 Generic flat plate PV Summary:

Table IV. 3 Generic flat plate PV Summary :

Quantity	Value	Units
Minimum Output	0	Kw
Maximum Output	42.0	kW
PV Penetration	182	%
Hours of Operation	4,399	hrs/yr
Levelized Cost	0.115	\$/kWh
Mean Output	9.74	kW
Mean Output	234	kWh/d
Capacity Factor	20.0	%
Total Production	85,299	kWh/yr

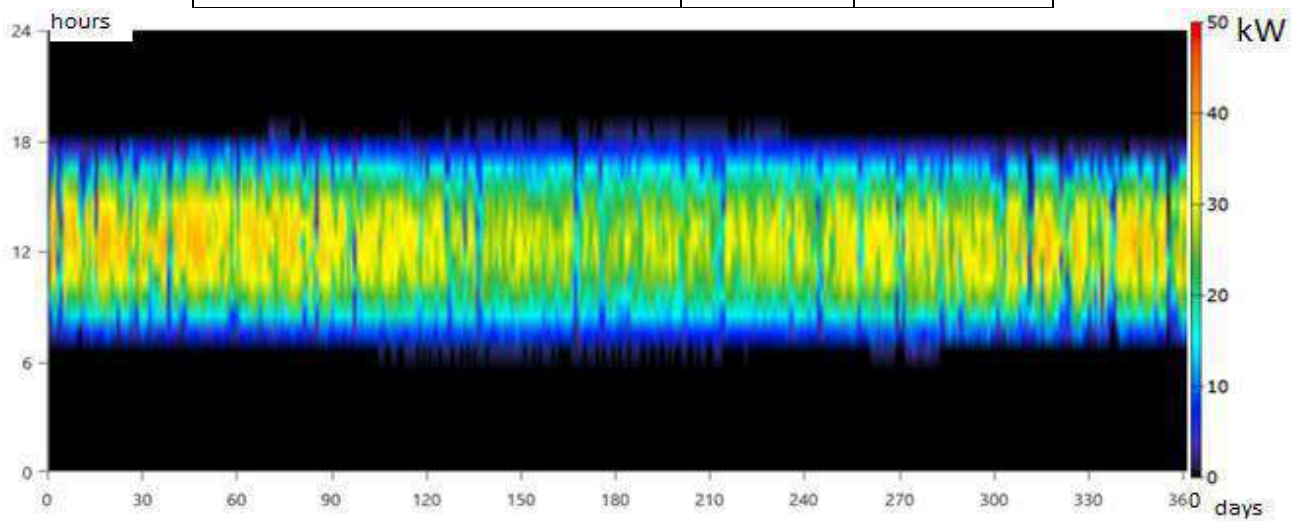


Fig IV. 33 PV modules Dmap

IV.2.3.3 Wind Turbine: Generic 1 kW

IV.2.3.3.1 Generic 1 kW Summary

Table IV. 4 Generic 1 kW Summary

Quantity	Value	Units
Minimum Output	0	kW
Maximum Output	1.00	kW
Wind Penetration	2.29	%
Hours of Operation	6,504	hrs/yr
Levelized Cost	0.551	\$/kWh
Total Rated Capacity	1.00	kW
Mean Output	0.123	kW
Capacity Factor	12.3	%
Total Production	1,075	kWh/yr

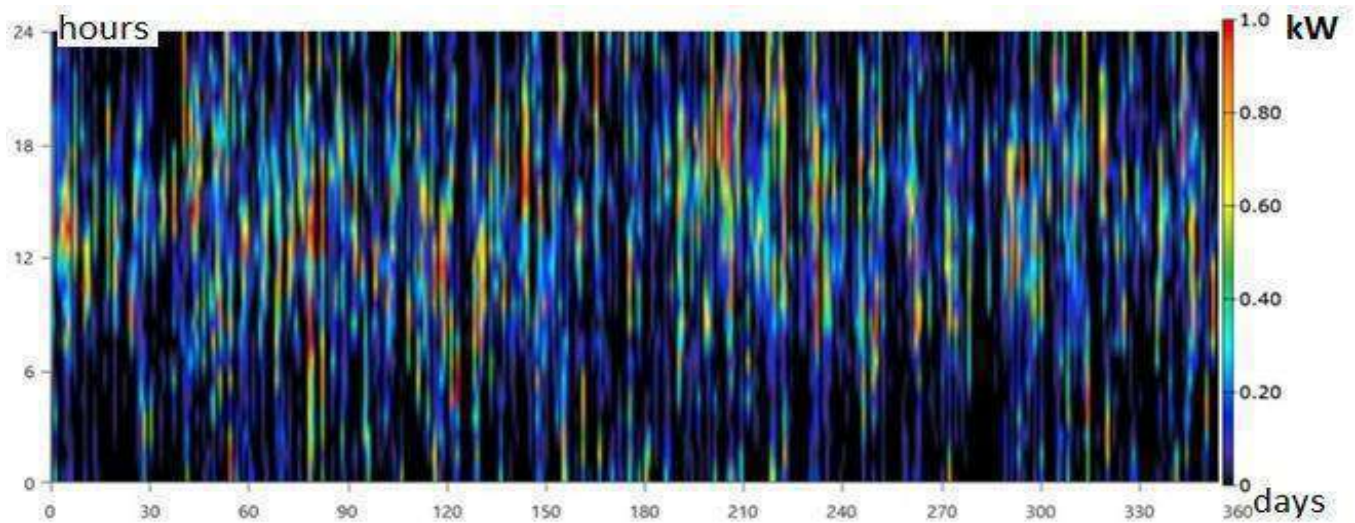


Fig IV. 34 Wind turbine Dmap

- Noticed from the wind Dmap pattern that the wind turbine provide almost the same amount of power during all the year days .
- Noticed from the table that wind penetration value is very low 2.29%

IV.2.3.4 Electrolyzer:

IV.2.3.4.1 Electrolyzer Summary:

Table IV. 5 electrolyzer summary

Quantity	Value	Units
Mean output	0.155	kg/hr
Minimum Output	0	kg/hr
Maximum Output	0.646	kg/hr
Total production	1,360	kg/yr
Specific consumption	46.4	kWh/kg
Rated capacity	30.0	kW
Mean input	7.20	kW
Minimum input	0	kW
Maximum input	30.0	kW
Total input energy	63,101	kWh/yr
Capacity Factor	24.0	%
Hours of operation	3,860	hr/yr

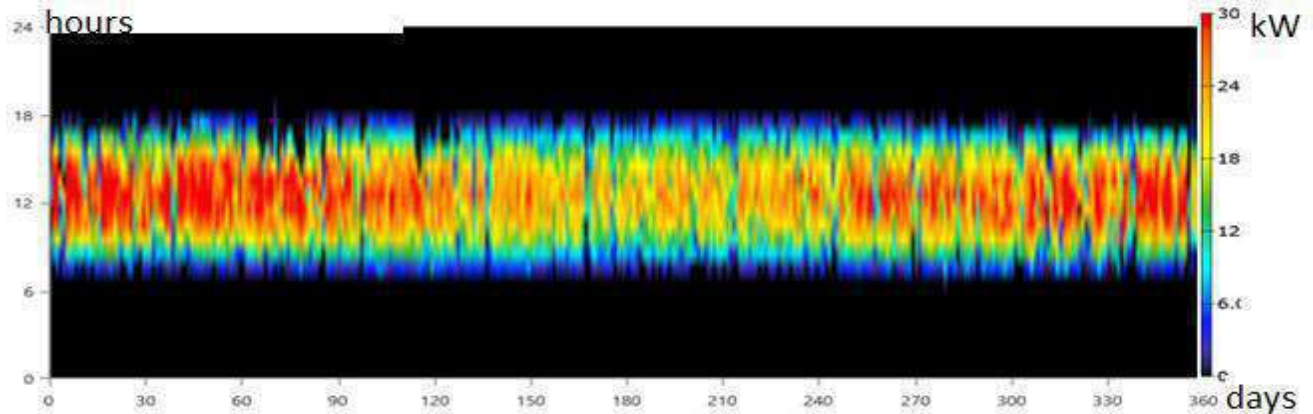


Fig IV. 35 Electrolyzer Dmap

IV.2.3.5 Hydrogen Tank:

IV.2.3.5.1 Hydrogen Tank Properties:

Table IV. 6 Hydrogen Tank Properties

Quantity	Value	Units
Hydrogen storage capacity	20.0	kg
Energy storage capacity	667	kWh
Tank autonomy	125	hr
Content at beginning of year	2.00	kg
Content at end of year	2.21	kg

Whats important here is the tank autonomy which indicates the power that the storage system can provide to the primary load without other power sources contribution.

Tank autonomy was calculated as 125hr or nearly 5 days and ¼ day and it's more than enough period to fix problems in the power sources.

NOTE:

Like battery bank case we can change the tank autonomy period by changing tank size.

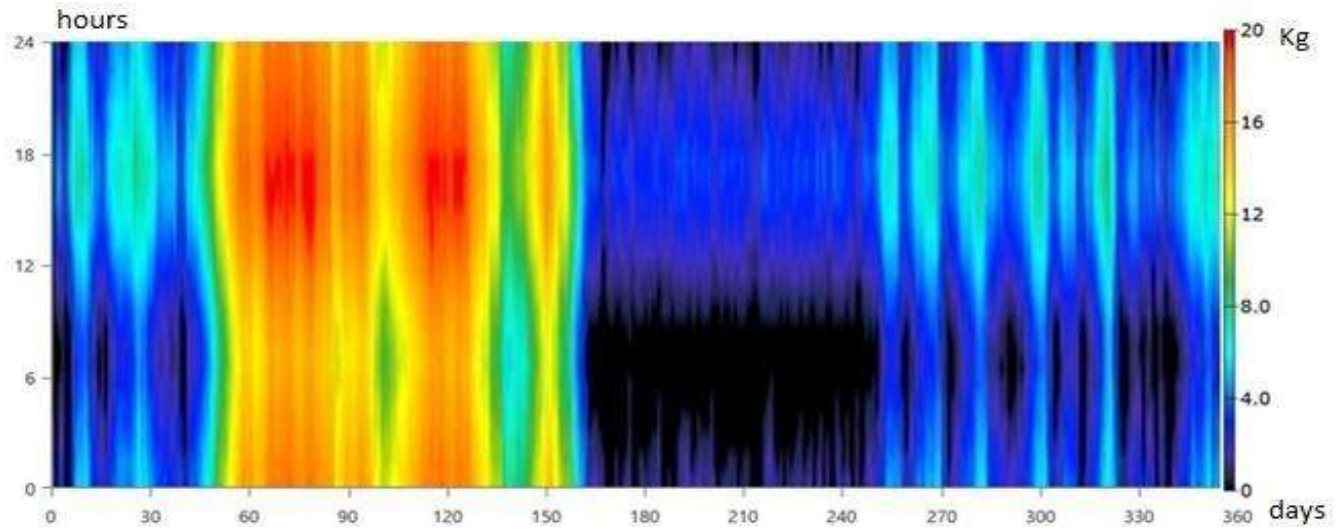


Fig IV. 36 Hydrogen tank Dmap

IV.2.3.5.2 Stored hydrogen Consumption Statistics

Table IV. 7 hydrogen Consumption Statistics

Quantity	Value	Units
Total fuel consumed	1,360	Kg
Avg fuel per day	3.73	kg/day
Avg fuel per hour	0.155	kg/hour

IV.2.4 Electrical Summary:

IV.2.4.1 Excess and Unmet:

Table IV. 8 excess and unmet energy

Quantity	Value	Units
Excess Electricity	1,275	kWh/yr
Unmet Electric Load	2,226	kWh/yr
Capacity Shortage	2,573	kWh/yr

As we can see from the figure 10 the value of the annual excess electricity is acceptable(1.17% from the total production) ,also our load could tolerate the values of the annual

capacity shortage and the unmet electric because we set maximum annual capacity shortage to be 10% and its about 5.5% ,and this indicates how really efficient is the load following dispatch strategy to control our system production/consumption.

IV.2.4.2 Production Summary:

Table IV. 9 Production Summary

Component	Production (kWh/yr)	Percent(%)
Generic flat plate PV	85,299	78.2
Fuel Cell	22,659	20.8
Generic 1 Kw	1,075	0.986
Total	109,034	100

As we can see from the table above the annual energy prduction PV production was based on the PV source(78.2%) then fuel cell production contribution was relatively good (20.8%) however the wind production is very low.

IV.2.5 System economical aspect:

IV.2.5.1 Project cost summary

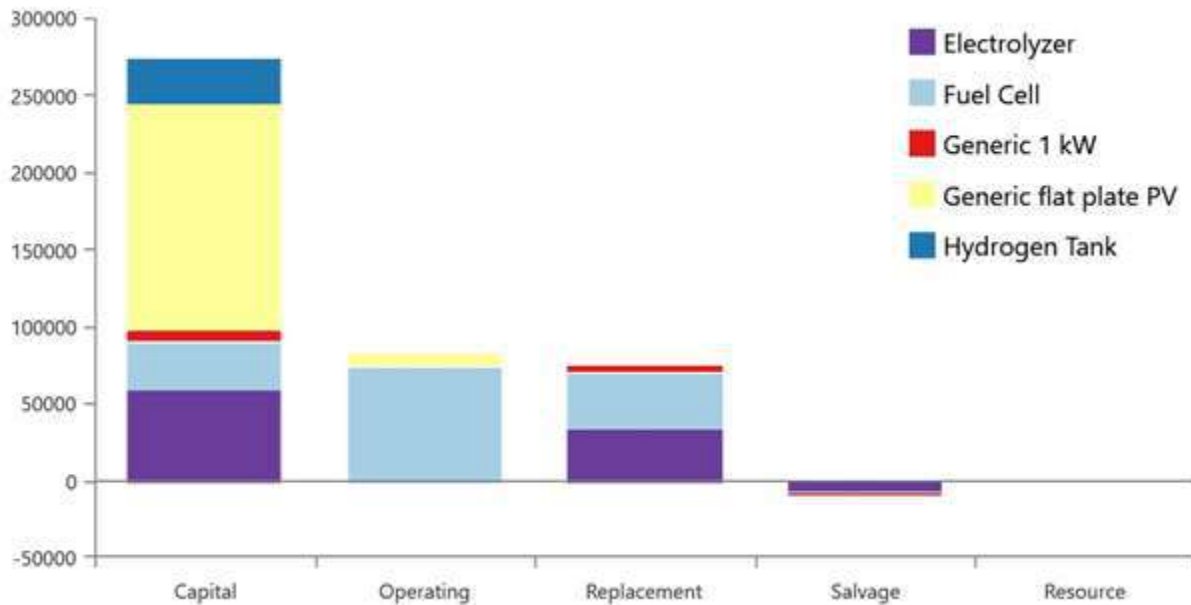


Fig IV. 37 Project cost summary

IV.2.5.1.1 Net Present Costs:

Table IV. 10 project NPC costs

Name	Capital	Operating	Replacement	Salvage	Resource	Total
Electrolyzer	\$60,000	\$0.00	\$33,695	-\$7,645	\$0.00	\$86,050
Fuel Cell	\$30,000	\$73,784	\$37,153	-\$831.41	\$0.00	\$140,106
Generic1 kW	\$7,000	\$1,103	\$3,243	-\$2,007	\$0.00	\$9,339
Generic flat plate PV	\$146,250	\$7,679	\$0.00	\$0.00	\$0.00	\$153,929
Hydrogen Tank	\$30,000	\$0.00	\$0.00	\$0.00	\$0.00	\$30,000
System	\$273,250	\$82,566	\$74,091	-\$10,483	\$0.00	\$419,424

As we could notice from the figure above that the largest cost of the project was initial Capital costs which were in the first year then some changes occurred regularly during the 25 years of the project, also noticed that Fuel cell operation and replacement costs were very high comparing to the initial costs, and that's what make fuel cells an expensive storage technique.

At the end of the project, there was a remaining value from wind turbine, electrolyzer and fuel cell of 10483\$ that counted as a revenue or salvage.

Interpretation :

The project TNPC were 419,424\$,furthermore the cost of energy would be 0.5962\$/kW all these results make our standalone hybrid power system comparative.

IV.2.6 PV/wind/FC based system VS diesel generator based system:

In order to compare between these systems we kept the same load and constraints

Here is some diesel genset based system results:

IV.2.6.1 Diesel generator Output:

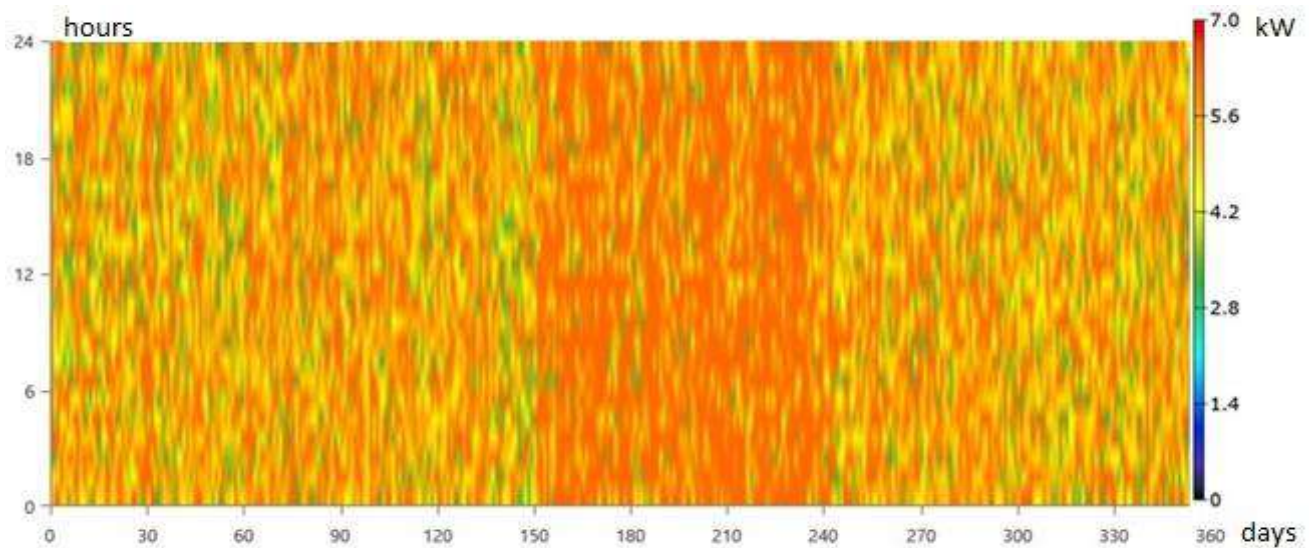


Fig IV. 38 diesel genset Dmap output

As we can see from the diesel genset Dmap the power production take values between 4 to nearly 7 kw all the year .

IV.2.6.2 Diesel genset based power System costs :

Table IV. 11 Net Present Costs

Name	Capital	Operating	Replacement	Salvage	Resource	Total
14kW Genset	\$7,000	\$57,956	\$61,928	-\$1,070	\$287,808	\$413,621
System Converter ac/dc	\$1,780	\$0.00	\$999.44	-\$226.77	\$0.00	\$2,552
System	\$8,780	\$57,956	\$62,927	-\$1,297	\$287,808	\$416,173
Levilized COE	0.594\$					

IV.2.6.3 Cost summary:

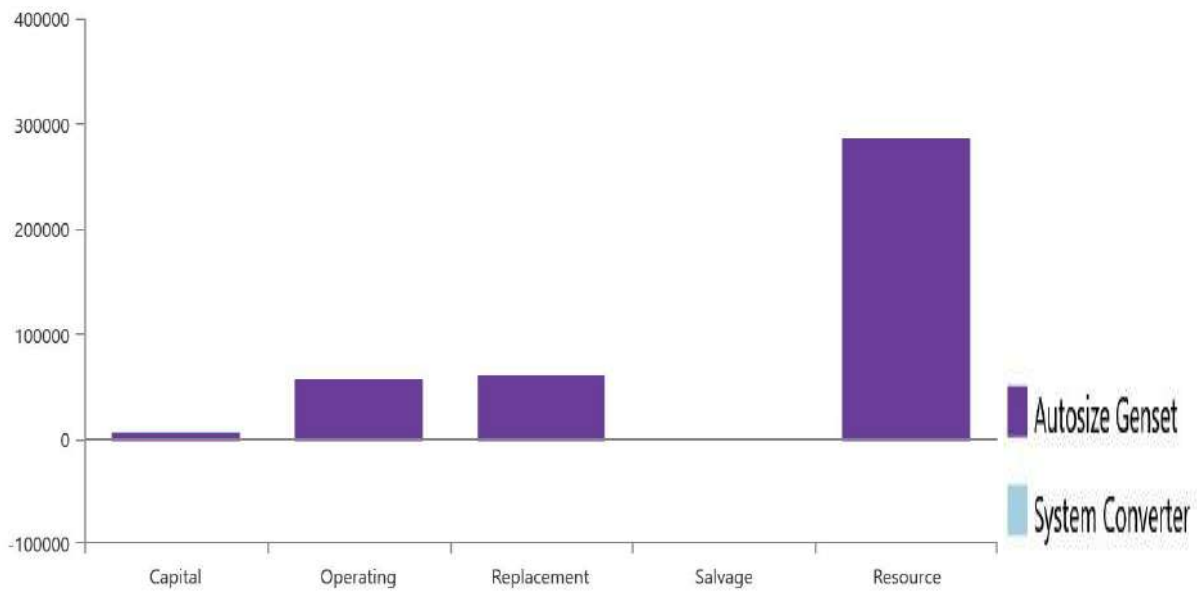


Fig IV. 39 cost summary

IV.2.6.4 Results Discussion:

As we can see:

A. Diesel genset system production output based totally on diesel generator ,in case of maintenance or replacement or diesel lack the entire system will stop working (no cellular network) and that why hybrid systems are good in this case (autonomy hours) .

B. The economic aspect comparison is based on these two costs:

a. The total net present cost

b. COE

They have almost the same compared to our renewable system (Renewables based system cost little bit greater)

C. on the contrary of the renewable hybrid system the operation and replacement cost is higher than the initial cost in case of diesel genset based system also it consumes a lot of fuel(diesel) which an exhausted resources and are the main air pollution producer (some countries apply penalties on that ,thus will increase system cost) .

Besides, if we count the particularity of the location in term of fuel transportation high cost (remote from the province 170kms bad situation road) this will rise the operation and replacement cost even more

These entire factors represent drawbacks for the diesel system

As a result its diesel system powering method fail against our renewable proposed system .

IV.3 Chapter summary

On this chapter we launch the simulation and optimization process ,also we discovered some featured functions and options that homer provide to the modeler to fully control and manage the power system.

Based on HOMER simulation and optimization results we selected our final optimal power system that is cost effective and satisfied our constraints.

CONCLUSIONS

Conclusion:

Based on HOMER method for simulation and optimization, we've suggested a new way to apply renewable clean electrical energy in remote areas cell sites and furthermore their other facilities.

We have found that the hybrid system (PV/Wind turbine) with fuel cell storage is the optimal system to solve the electrification problems in the saharien remote areas.

The system required components are followed:

- 49kW PV array
- 1kW wind turbine
- 10kW Fuel cell generator
- 30kW Electrolyzer
- 20Kg Hydrogen tank

We found that our system levelized cost of energy (LCOE) was reasonable 0.5962 \$/kWh whereas total net present cost (NPC) was 419,423.74\$.

And the total annual energy output is 109,034 kWh / year, were PV Solar panels produce the highest amount of energy.

On the other hand we studied diesel generator system alone to compare with our system and we've got almost the same cost values but the renewable system is show more reliability. Our system is an environmentally friendly energy source that contributes to reducing greenhouse gas emissions, unlike the diesel system.

In our study, the amount of greenhouse gas emissions from diesel generator which greatly increases the appearance of global warming in the atmosphere.

- ❖ The diesel generator system Carbon dioxide is released 47,826 kg/year (CO₂), Unlike the our system where weren't any emission of the carbon dioxide
- ❖ The diesel generator system Carbon monoxide is released 301 kg/year (CO), unlike the our renewable system is released 8.84 kg/year

Finally ,after presenting all possible economical and technical specifications of our system , we could say that we succeed in finding an optimal design for a reliable renewable energy based system combined of PV, Wind sources and the fuel cell for the compensation and the backup, this system is also cost effective

Outlooks:

- ✓ Obtain renewable energy technology components accurate local cost (in Algeria).
- ✓ Create our own dispatch strategy based on one of the optimization algorithm using HOMER Matlab link feature .
- ✓ Developing a new way to estimate an accurate load consumption profile.
- ✓ Contribute in update wind and solar resources database especially in our big dessert.

Appendices

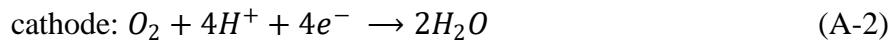
Appendix A: Fuel cell full modeling [27]

Conceptualization of the Modeling Technique

This study is focused on the theoretical mathematical model that can be used to quantify the performance of a fuel cell as a function of operating parameters. The mathematical model will consist of electrochemical, heat energy and exergy analysis components. The following assumptions were made in developing the predictive model:

- (i) There is incomplete utilization of the fuel and oxidant gases during the reaction process.
- (ii) The voltage losses encountered are activation polarization, ohmic polarization, and concentration polarization.
- (iii) The enthalpy calculations are based on standard temperature.
- (iv) The heat losses in the system are by natural convection, forced convection, and radiation.

Equations (A-1)–(A-3) represent the reactions taking place in a typical PEMFC system :



The actual (or net) output voltage of the PEMFC, V_{cell} as a function of current, temperature, partial pressure of reactant, and membrane humidity can be expressed as follows:

$$V_{cell} = E_{Nernst} - \eta_{act} - \eta_{ohmic} - \eta_{conc} \quad (\text{A-4})$$

Where E_{Nernst} is the thermodynamic equilibrium potential or open circuit voltage and η_{act} , η_{ohmic} , and η_{conc} are activation, ohmic, and concentration overvoltages, respectively. Other names for overvoltages are polarization or losses, and they represent voltage drop.

Appendix A

The reversible cell voltage or thermodynamic potential is the maximum voltage attained from a fuel cell at thermodynamic equilibrium which can be obtained by applying the Nernst equation as shown as follows:

$$E_{Nernst} = V^{\circ} + \frac{RT}{nF} \ln \left(\frac{p_{H_2} \sqrt{p_{O_2}}}{p_{H_2O}} \right) \quad (A-5)$$

Where V° is the standard state reference potential (298.15 K and 1 atm) at unit activity, p_{H_2} , p_{O_2} and, p_{H_2O} are partial pressures of hydrogen, oxygen, and water, respectively, R is the universal gas constant (8.314 J/mole K), T is the cell operating temperature (K), F is the Faraday constant (96,485 C/mole), and n represents the number of moles of electrons transferred, having a value of 2.

Equation (A-4) shows that part of the voltage is lost in driving the chemical reaction at the electrodes. This lost voltage is known as activation overvoltage (η_{act}) which occurs at both the anode and cathode. Activation overvoltage is however more predominant at cathode since the hydrogen oxidation is faster than oxygen reduction. A parametric equation for representing activation overvoltage as proposed by Uma is shown in the following equation:

$$\eta_{act} = \left[\xi_1 + \xi_2 T + \xi_3 T [\ln(c^*_{O_2})] + \xi_4 T [\ln(i)] \right] \quad (A-6)$$

The values of the parametric coefficients ξ_1 , ξ_2 , ξ_3 , and ξ_4 are determined using linear regression analysis. These values are

$$\xi_1 = -0.948$$

$$\xi_2 = 0.00286 + 0.0002(A) + 4.3 \times 10^{-5} \ln(c^*_{H_2})$$

$$\xi_3 = 7.6 \times 10^{-5}$$

$$\xi_4 = -1.93 \times 10^{-4} \quad (A-7)$$

where $c^*_{H_2}$ and $c^*_{O_2}$ are concentrations of hydrogen and oxygen, respectively, at the reaction sites, while A is the active cell area.

Appendix A

The concentrations of hydrogen and oxygen at the electrode-membrane interface can be determined from Henry's law equation of the forms expressed in the following two equations:

$$c^*_{H_2} = p_{H_2} 9.174 \times 10^{-7} \exp\left(\frac{-77}{T}\right) \quad (\text{A-8})$$

$$c^*_{O_2} = p_{O_2} 1.97 \times 10^{-7} \exp\left(\frac{498}{T}\right) \quad (\text{A-9})$$

Substituting the values of the parametric coefficients into (A-6), we obtain the expression in the following equation:

$$\eta_{act} = - \left[-0.948 + \left\{ 0.00286 + 0.0002 \ln(A) + 4.3 \times 10^{-5} \ln(c^*_{H_2}) \right\} T + \left\{ 7.6 \times 10^{-5} T \ln c^*_{O_2} - 1.93 \times 10^{-4} T \ln i \right\} \right] \quad (\text{A-10})$$

The voltage loss as a result of resistance to the flow of electrons through the electrodes and various interconnections and resistance to the flow of ions through the electrolyte is known as ohmic overvoltage (η_{ohmic}) which can be expressed as follows:

$$\eta_{ohmic} = iR = i(R_{electronic} + R_{ionic}) \quad (\text{A-11})$$

It has been reported that the resistance to flow of ions (R_{ionic}) is predominant; hence, its contribution to ohmic overvoltage is more significant than the resistance to the flow of electrons ($R_{electronic}$). The ionic resistance is a function of the membrane water content which in turn is a function of temperature and current. Hence, the ionic resistance can be expressed as follows:

$$R_{ionic} = \frac{r_M l_{mem}}{A} \quad (\text{A-12})$$

Where r_M is the membrane resistivity l_{mem} , is the membrane thickness, and A is the active cell area. The membrane resistivity in (A-12) was correlated by Rezazadeh et al. as shown in the following equation:

$$r_M = \frac{181.6 [1 + 0.03(i/A) + 0.062(T/303)^2 (i/A)^{2.5}]}{[\lambda - 0.634 - 3(i/A)] \exp [4.18((T-303)/T)]} \quad (\text{A-13})$$

Substituting the expression in (A-13) into (A-12), we obtain the following:

Appendix A

$$R_{ionic} = \frac{\left(\frac{181.6[1+0.03(i/A)+0.062(T/303)^2(i/A)^{2.5}]}{[\lambda-0.634-3(i/A)]\exp[4.18((T-303)/T)]} \right) l_{mem}}{A} \quad (A-14)$$

Substituting (A-14) into (A-11), we also obtain η_{ohmic} expression as follows:

$$\eta_{ohmic} = i \left\{ \frac{\left(\frac{181.6[1+0.03(i/A)+0.062(T/303)^2(i/A)^{2.5}]}{[\lambda-0.634-3(i/A)]\exp[4.18((T-303)/T)]} \right) l_{mem}}{A} \right\} \quad (A-15)$$

The concentration overvoltage (η_{conc}) is another factor that can also affect the performance of the fuel cell. As reactant is consumed at the electrode by electrochemical reaction, there is a loss of potential due to the inability of the surrounding material to maintain the initial concentration of the bulk fluid (formation of concentration gradient). Several processes that may contribute to concentration polarization include slow diffusion in the gas phase in the electrode pores, solution/dissolution of reactants/products into/out of the electrolyte, or diffusion of reactants/products through the electrolyte to/from the electrochemical reaction site. Concentration overvoltage (or polarization) is also called mass transportation losses. However, at practical current densities, slow transport of reactants/products to/from the electrochemical reaction site is a major contributor to concentration polarization. Concentration overpotential can be expressed as follows:

$$\eta_{conc} = -B \ln \left(1 - \frac{J}{J_{max}} \right) \quad (A-16)$$

where B is a parametric coefficient and J represents the actual current density of the cell (A/cm^2). Substituting (A-5), (A-10), (A-15), and (A-16) into (A-4) gives a generalized equation for voltage output of the cell, V_{cell} , as follows:

Appendix A

$$\begin{aligned}
 V_{\text{cell}} = & \left\{ V^{\circ} + \frac{RT}{nF} \ln \left(\frac{p_{H_2} \sqrt{p_{O_2}}}{p_{H_2O}} \right) \right\} - 0.948 \\
 & + \{0.00286 + 0.0002 \ln(A) + 4.3 \times 10^{-5} \ln(c^*_{H_2})\} T \\
 & + \{7.6 \times 10^{-5} T [\ln(c^*_{O_2})]\} - 1.93 \\
 & \times 10^{-4} T [\ln(i)] \\
 & - i \left\{ \frac{\left(\left(\frac{181.6 [1 + 0.03(i/A) + 0.062(T/303)^2 (i/A)^{2.5}]}{[\lambda - 0.634 - 3(i/A)] \exp[4.18((T - 303)/T)]} \right) l_{mem} \right)}{A} \right\} \\
 & + B \ln \left(1 - \frac{J}{J_{max}} \right) \tag{A - 17}
 \end{aligned}$$

Equation (A-17) is the predictive model expression for the voltage output from PEMFC as a function of the operating parameters for a single fuel cell.

The actual efficiency of the fuel cell can be obtained from the expression shown as follows:

$$\text{Cell efficiency} = \frac{V_{\text{Cell}}}{V_C} \times 100 \tag{A - 18}$$

Where V_C is the actual voltage having a value of about 1.23 V, and V_{Cell} is determined from (A-17).

In practice, not all the reactants going into the system react completely as some fractions of the fuel pass through the cell without taking part in energy production process; hence, fuel utilization term is introduced in calculating the proton exchange membrane fuel cell efficiency.

The fuel utilization coefficient is given as follows:

$$\delta_f = \frac{\text{mass of fuel } (H_2) \text{ reacted in the cell}}{\text{mass of fuel } (H_2) \text{ input into the cell}} \tag{A - 19}$$

If (A-19) is substituted into (A-18), it gives the following expression:

$$\text{Cell efficiency} = \frac{V_{\text{Cell}}}{V_C} \times 100 \tag{A - 20}$$

Appendix A

2.1. Mass Balance for the PEMFC

As a requisite to carrying out energy balance for the PEM fuel cell, material balance becomes necessary. The mass balance was performed based on the inflow and outflow of the reactants (H_2 and O_2) into and out of the fuel cell system as shown in Figure 1.

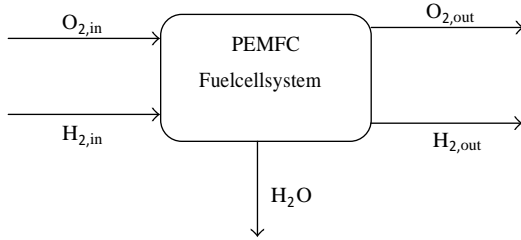


Figure 1: Schematic mass balances for the PEMFC.

Considering the fact that not all reactants that entered the fuel cell were utilized, the component material balance for hydrogen and oxygen can be written as follows:

$$m_{H_2,in} = m_{H_2,react} + m_{H_2,out} \quad (A - 21)$$

$$m_{O_2,in} = m_{O_2,react} + m_{O_2,out} \quad (A - 22)$$

Where $m_{H_2,in}$ and $m_{O_2,in}$ are the mass flow rates of hydrogen and oxygen entering the PEM fuel cell, respectively. In addition, $m_{H_2,out}$ and $m_{O_2,out}$ are the mass flow rates of hydrogen and oxygen from PEM fuel cell, respectively. They represent hydrogen purged out of the fuel cell and the unreacted oxygen, respectively. The mass balance of the reactants (O_2 and H_2) requires the essential electrochemistry principles to calculate the hydrogen and oxygen consumption rates, $m_{H_2,react}$ and $m_{O_2,react}$, and the water production, $m_{H_2O,out}$, as functions of current density i (A/cm^2) and Faraday's constant.

Hydrogen reacts on the anode side; thus the consumption rate of hydrogen is given as

$$m_{H_2,react} = \zeta_A M_{H_2} \frac{IA_{cell}}{2F} \times 10^{-3} \quad (A - 23)$$

Appendix A

where ζ_A stands for the anode stoichiometry, M_{H_2} is the molecular weight of hydrogen, i is the current density, A_{cell} is the effective area of the cell, and F is Faraday's constant. Similarly, the consumption rate of oxygen can be calculated from the following equation :

$$m_{O_2,react} = \zeta_C M_{O_2} \frac{JA_{cell}}{2F} \times 10^{-3} \quad (A - 24)$$

Where ζ_C represents the cathode stoichiometry and M_{O_2} is the molecular weight of oxygen.

Assuming water produced from the fuel cell to be liquid, water production rate can be expressed as follows:

$$m_{H_2O,out} = M_{H_2O} \frac{JA_{cell}}{2F} \times 10^{-3} \quad (A - 25)$$

Where M_{H_2O} represents the molecular weight of water.

Hydrogen and oxygen which leave the system unutilized, $m_{H_2,out}$ and $m_{O_2,out}$, respectively, will be determined from (A – 21) and (A – 22) as follows:

$$m_{H_2,out} = m_{H_2,in} - m_{H_2,react} \quad (A - 26)$$

Substituting for $m_{H_2,react}$ gives

$$m_{H_2,out} = m_{H_2,in} - \zeta_A M_{H_2} \frac{JA_{cell}}{2F} \times 10^{-3} \quad (A - 27)$$

Similarly,

$$m_{O_2,out} = m_{O_2,in} - m_{O_2,react} \quad (A - 28)$$

$$m_{O_2,out} = m_{O_2,in} - \zeta_C M_{O_2} \frac{JA_{cell}}{2F} \times 10^{-3} \quad (A - 29)$$

Larminie and Dicks [31] give alternate equations for calculating the inlet mass flow rates of hydrogen and oxygen as shown in the following equations:

$$m_{O_2,in} = \text{oxygen}_{in} = 3.57 \times 10^{-7} \left(\frac{\lambda_s \times W_{net}}{V_{Cell}} \right) \quad (A - 30)$$

Appendix A

$$m_{\text{H}_2,\text{in}} = \text{hydrogen}_{\text{in}} = 1.05 \times 10^{-8} \left(\frac{W_{\text{net}}}{V_{\text{Cell}}} \right) \quad (\text{A} - 31)$$

Similarly, mass flow rates of unused oxygen and product water are given in expression in the following equations:

$$m_{\text{O}_2,\text{out}} = \text{oxygen}_{\text{out}} = 3.57 \times 10^{-7} \left(\frac{\lambda_s \times W_{\text{net}}}{V_{\text{Cell}}} \right) - 8.29 \times 10^{-8} \left(\frac{W_{\text{net}}}{V_{\text{Cell}}} \right) \quad (\text{A} - 32)$$

$$m_{\text{H}_2\text{O},\text{out}} = \text{water}_{\text{out}} = 9.34 \times 10^{-8} \left(\frac{W_{\text{net}}}{V_{\text{Cell}}} \right) \quad (\text{A} - 33)$$

Where λ_s is the stoichiometry of oxygen.

2.2. Energy Analysis for the PEMFC

The conservation law of energy which is the first law of thermodynamics is used to analyze the energy model of the proton exchange membrane fuel cell. The energy balance around a fuel cell is based on the energy absorbing/releasing processes (power produced, reactions, and heat loss) that occur in the cell. As a result, the energy balance varies for the different types of cells because of the differences in reactions that occur according to the cell types.

The cell energy balance states that the enthalpy flow of reactants entering the cell will be equal to the enthalpy flow of the products leaving the cell plus the sum of three terms, namely, (i) the net heat generated by physical and chemical processes within the cell, (ii) the dc power output from the cell, and (iii) the rate of heat loss from the cell to its surroundings. The energy balance according to the heat flow into and out of the cell as shown in Figure 2 can be represented mathematically as follows:

$$Q_{\text{input}} - Q_{\text{output}} - Q_{\text{acc}} = 0 \quad (\text{A} - 34)$$

where Q_{input} and Q_{output} are the total heat input and output, respectively, and Q_{acc} is the heat accumulation which is the net heat generated by physical and chemical processes within the cell.

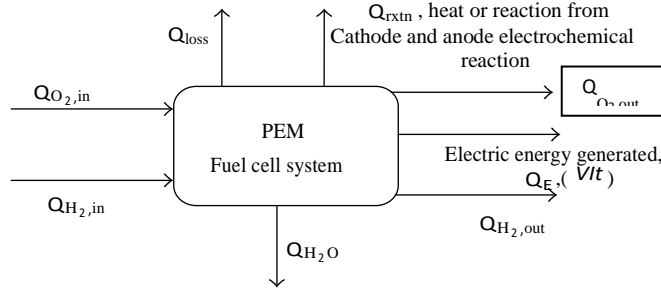


Figure 2: Schematic energy (enthalpy) balances for the PEMFC.

By replacing Q_{acc} in (A – 34) with Q_{net} and rearranging, we obtain the following expression:

$$Q_{net} = Q_{input} - Q_{output} \quad (A - 35)$$

From the schematic shown in Figure 2, the total heat input into the system is

$$Q_{input} = Q_{H_2,in} + Q_{O_2,in} \quad (A - 36)$$

where $Q_{H_2,in}$ and $Q_{O_2,in}$ are the heats from the reactant feeds. Similarly, the total heat output from the system is as shown as follows:

$$Q_{output} = Q_{H_2,out} + Q_{O_2,out} + Q_{H_2O} + Q_{rxtn} + Q_E + Q_{loss} \quad (A - 37)$$

From (A – 37), $Q_{H_2,out}$ and $Q_{O_2,out}$ are the heats from the unreacted hydrogen and oxygen, respectively, Q_{H_2O} is the heat from water produced, Q_{rxtn} is the heat of reaction from cathode and anode electrochemical reaction, Q_{loss} is the heat loss to the surroundings, and Q_E is the electrical energy ($V_{Cell} \times It$) generated.

The heat generated by the fuel cell system is transferred through the stack by conduction, which then dissipates into the surroundings using natural convection, forced convection, and radiation. Hence, the three heat transfer mechanisms play important roles to transfer the heat from the fuel cell stack to the ambient. In addition, some heat is carried away from the fuel cell stack by the product gases and water. Heat lost termed Q_{loss} from the fuel cell can be represented as follows:

Appendix A

$$Q_{\text{loss}} = Q_{\text{nc}} + Q_{\text{fcn}} + Q_{\text{rad}} \quad (\text{A} - 38)$$

where Q_{nc} , Q_{fcn} , and Q_{rad} are heat losses via natural convection, forced convection, and radiation, respectively. The considering a fuel cell slab of solid material of area expressions for Q_{cond} , Q_{nc} , Q_{fcn} , and Q_{rad} can be obtained by considering a fuel cell slab of solid material of area A located between two large parallel plates at distance Y apart; the rate of heat flow by conduction per unit area is given by Fourier expression as follows:

$$\frac{Q_{\text{cond}}}{A} = K \frac{\Delta T}{Y} \quad (\text{A} - 39)$$

That is, the rate of heat flow per unit area is proportional to the temperature decrease over the distance Y . The constant of proportionality K is the thermal conductivity of the slab. ΔT is given as $(T_1 - T_0)$, where T_0 and T_1 are the initial temperature and the temperature at a steady-state condition of heat flow across the slab.

Q_{nc} and Q_{fcn} are calculated separately from (A – 40) and (A – 41), respectively:

$$Q_{\text{nc}} = h_{\text{nc}} A_{\text{FC}} (T_{\text{FC}} - T_0) \quad (\text{A} - 40)$$

$$Q_{\text{fcn}} = m_{\text{coolant}} C_{p,\text{air}} (T_{\text{coolant, out}} - T_0) \quad (\text{A} - 41)$$

Air is used as coolant in fuel cells; h_{nc} is the natural convective heat transfer coefficient; A_{FC} is the total heat transfer area of the fuel cell; it can be estimated from the dimensions of the fuel cell system. T_0 is the ambient temperature which is assumed to be the dead state temperature of 298 K.

For nonblack surfaces at temperature T , the emitted energy flux is given by *Stefan-Boltzmann law* as

$$Q_{\text{rad}} = \varepsilon \sigma A_{\text{FC}} (T_{\text{FC}}^A - T_0^A) \quad (\text{A} - 42)$$

where T is the absolute temperature and A_{FC} is the total heat surface area of the fuel cell system. The Stefan-Boltzmann constant σ has been found to have the value of $5.67 \times 10^{-8} \text{ W/m}^2 \text{ K}^4$, and ε is the emissivity having standard values for various materials.

Substituting (A – 36) to (A – 38) and (A – 40) to (A – 42) into (A – 35) will yield

Appendix A

$$Q_{\text{net}} = Q_{\text{H}_2,\text{in}} + Q_{\text{O}_2,\text{in}} - Q_{\text{H}_2,\text{out}} - Q_{\text{O}_2,\text{out}} - Q_{\text{H}_2\text{O}} - Q_{\text{rxtn}} - Q_E \quad (\text{A } 43)$$

$$-h_{\text{nc}}A_{\text{FC}}(T_{\text{FC}} - T_0) - m_{\text{coolant}} C_{p,\text{air}}(T_{\text{coolant},\text{out}} - T_0) - \varepsilon\sigma A_{\text{FC}}(T_{\text{FC}}^A - T_0^A)$$

Equation (A – 43) can be rewritten in terms of enthalpies to yield the following equation:

$$Q_{\text{net}} = \Delta H_{\text{H}_2,\text{in}} + \Delta H_{\text{O}_2,\text{in}} - \Delta H_{\text{H}_2,\text{out}} - \Delta H_{\text{O}_2,\text{out}} - \Delta H_{\text{H}_2\text{O}} - \Delta H_{\text{rxtn}} - Q_E \quad (\text{A } 44)$$

$$-h_{\text{nc}}A_{\text{FC}}(T_{\text{FC}} - T_0) - m_{\text{coolant}} C_{p,\text{air}}(T_{\text{coolant},\text{out}} - T_0) - \varepsilon\sigma A_{\text{FC}}(T_{\text{FC}}^A - T_0^A)$$

where ΔH_{O_2} , ΔH_{H_2} , and $\Delta H_{\text{H}_2\text{O}}$ are the enthalpies of oxygen, hydrogen, and water, respectively, and ΔH_{rxtn} is the enthalpy of reaction.

The electrical energy dissipated Q_E is related to the net output voltage V_{Cell} by

$$Q_E = V_{\text{Cell}} \times It \quad (\text{A } 45)$$

where I is the current and t is the duration of operation. Equation (A – 44) can be rearranged to obtain

$$Q_{\text{net}} = \Delta H_{\text{H}_2,\text{in}} + \Delta H_{\text{O}_2,\text{in}} - \Delta H_{\text{H}_2,\text{out}} - \Delta H_{\text{O}_2,\text{out}} - \Delta H_{\text{H}_2\text{O}} - \Delta H_{\text{rxtn}} - V_{\text{Cell}} \times It$$

$$-h_{\text{nc}}A_{\text{FC}}(T_{\text{FC}} - T_0) - m_{\text{coolant}} C_{p,\text{air}}(T_{\text{coolant},\text{out}} - T_0) - \varepsilon\sigma A_{\text{FC}}(T_{\text{FC}}^A - T_0^A) \quad (\text{A } 46)$$

The enthalpy of reaction term, ΔH_{rxtn} , in the energy balance equation is computed as follows:

$$\Delta H_{\text{rxtn}} = \Delta H_{\text{rxtn}}^\circ + \int_{298}^T (\Delta C_p) dT. \quad (\text{A } 47)$$

Upon integration of (A – 47), ΔH_{rxtn} becomes

$$\Delta H_{\text{rxtn}} = \Delta H_{\text{rxtn}}^\circ + \Delta C_p(T - 298) \quad (\text{A } 48)$$

Where: $\Delta H_{\text{rxtn}}^\circ = (n_i \Delta H_{\text{fi}}^\circ)_{\text{prdcts}} - (n_i \Delta H_{\text{fi}}^\circ)_{\text{rxtns}}$.

For the PEMFC, where: $2\text{H}_2 + \text{O}_2 \rightarrow 2\text{H}_2\text{O}$, 2 moles of H_2 and 1 mole of O_2 give 2 moles of H_2O :

Appendix A

$$\Delta H^{\circ}_{\text{rxtn}} = \left(2 \times \Delta H^{\circ}_{\text{f}_{\text{H}_2\text{O}}}\right)_{\text{prdcts}} - \left[\left(2 \times \Delta H^{\circ}_{\text{f}_{\text{H}_2}}\right) + \left(1 \times \Delta H^{\circ}_{\text{f}_{\text{O}_2}}\right)\right]_{\text{rxtnnts}} \quad (\text{A}-49)$$

And also from the reaction stoichiometry,

$$\Delta C_p = \left(2 \times \Delta C_{\text{p}_{\text{H}_2\text{O}}}\right)_{\text{prdcts}} - \left[\left(2 \times \Delta C_{\text{p}_{\text{H}_2}}\right) + \left(1 \times \Delta C_{\text{p}_{\text{O}_2}}\right)\right]_{\text{rxtnnts}} \quad (\text{A}-50)$$

Therefore, the energy efficiency of the PEMFC system is

$$\eta_{\text{energy, system}} = \frac{\dot{W}_{\text{net}}}{\text{HHV}_{\text{H}_2} \times m_{\text{H}_2, \text{in}}} \quad (\text{A}-51)$$

Higher heating value of a fuel (HHV) is the negative value of the standard heat of combustion when water in the combustion products is in form of a liquid. Here, is the higher heating value of hydrogen, \dot{W}_{net} ($V_{\text{Cell}} \times I_t$) is the net power production of the fuel cell system, and $m_{\text{H}_2, \text{in}}$ is the mass flow rate of hydrogen to the PEMFC.

Exergy Analysis

The flow exergy of a substance refers to the theoretically obtainable work when that substance is brought to total equilibrium with the local environment. It can be divided into thermomechanical and chemical flow exergies. Hence, the total exergy rate can be written as

$$\hat{E} = \hat{E}_{\text{tm}} + \hat{E}_{\text{CH}} \quad (\text{A}-52)$$

The thermomechanical exergy is also known as physical exergy, and it represents the deviation in temperature and pressure between the flowing matter and the ambient. It also includes the kinetic and potential exergies. However, the chemical exergy represents the deviation in chemical composition between the flowing matter and the local environment. Therefore, (A-52) becomes

$$\hat{E} = \hat{E}_{\text{ke}} + \hat{E}_{\text{pe}} + \hat{E}_{\text{tm}} + \hat{E}_{\text{CH}} \quad (\text{A}-53)$$

Amir et al. also give the specific total exergy (J/kg) as the sum of kinetic exergy, potential exergy, thermomechanical exergy, and chemical exergy as:

$$e = e_{\text{ke}} + e_{\text{pe}} + e_{\text{tm}} + e_{\text{CH}} \quad (\text{A}-54)$$

Appendix A

where $e = \hat{E}/m$, \hat{E} is the total exergy rate (J/hr), and represents the mass flow rate (kg/hr). Therefore, (A –54) becomes:

$$\hat{E} = me_{ke} + me_{pe} + me_{tm} + me_{CH} \quad (A -55)$$

The specific kinetic exergy term, e_{ke} , is expressed as:

$$e_{ke} = \frac{1}{2} v^2 \quad (A -56)$$

where v is the velocity relative to the earth surface (m/s); and the specific potential exergy term, e_{pe} , is given by:

$$e_{pe} = gZ \quad (A -57)$$

Where g is the earth gravity (m/s^2) and Z is the stream altitude above the sea level (m).

The thermomechanical exergy shown in (A –54) can be simplified as a function of fuel cell operating temperature and pressure as:

$$e_{tm} = (h - h_0) - T_0(s - s_0) \quad (A -58)$$

Where h_0 and s_0 represent the specific enthalpy (J/kg) and entropy (J/kg·K) at standard conditions, respectively; $(h - h_0)$ and $(s - s_0)$ are changes in enthalpy and entropy, respectively.

Meanwhile, Masanori and Abdelaziz expressed the specific molar chemical exergy of component present in the environment at partial pressure $P_{00,i}$ as

$$e_{CH} = RT_0 \ln \left(\frac{P_0}{P_{00,i}} \right) \quad (A -59)$$

Where P_0 is the environmental pressure (usually taken as 1 atm) and $P_{00,i}$ is the partial pressure of the reference component and R is the ideal gas constant.

Hence, substituting (A – 56) to (A – 59) into (A – 54) yields an expression for the specific total exergy; thus,

$$e = \frac{1}{2} v^2 + gZ + [(h - h_0) - T_0(s - s_0)] + RT_0 \ln \left(\frac{P_0}{P_{00,i}} \right) \quad (A -60)$$

Appendix A

The specific thermomechanical exergy term $(h - h_0) - T_0(s - s_0)$ of (A -58) can be evaluated further as a function of fuel cell operating condition:

$$(h - h_0) = \int_{T_0}^T C_p(T) dT = C_p (T - T_0) \quad (\text{A -61})$$

$$(s - s_0) = \int_{T_0}^T \frac{C_p}{T} dT = \int_{P_0}^P \left(\frac{\partial V}{\partial T} \right) dP \quad (\text{A -62})$$

Based on ideal gas assumption, $P \partial V = R \partial T$, so that

$$\frac{\partial V}{\partial T} = \frac{R}{P} \quad (\text{A -63})$$

Where R is the universal gas constant; substituting (A -63) into (A -62) gives

$$(s - s_0) = \int_{T_0}^T \frac{C_p}{T} dT = \int_{P_0}^P \left(\frac{R}{P} \right) dP \quad (\text{A -64})$$

Integrating (A -63) yields

$$(s - s_0) = C_p \ln \left(\frac{T}{T_0} \right) - R \ln \left(\frac{P}{P_0} \right) \quad (\text{A -65})$$

Specific heats at constant pressure, C_p , and at constant volume, C_v , are related to R as

$$C_p = C_v + R \quad \text{or} \quad R = C_p - C_v \quad (\text{A -66})$$

Substituting for R in (A -65),

$$(s - s_0) = C_p \ln \left(\frac{T}{T_0} \right) - (C_p - C_v) \ln \left(\frac{P}{P_0} \right) \quad (\text{A -67})$$

Rearrange (A -67) to obtain

$$(s - s_0) = C_p \left[\ln \left(\frac{T}{T_0} \right) - \left(1 - \frac{C_v}{C_p} \right) \ln \left(\frac{P}{P_0} \right) \right] \quad (\text{A -68})$$

C_v/C_p can be expressed in terms of the specific heat ratio, k ; thus,

$$k = \frac{C_p}{C_v} \quad \text{or} \quad \frac{1}{k} = \frac{C_v}{C_p} \quad (\text{A -69})$$

Hence, (A -68) becomes

Appendix A

$$(s - s_0) = C_p \left[\ln \left(\frac{T}{T_0} \right) - \left(\frac{k-1}{k} \right) \ln \left(\frac{P}{P_0} \right) \right] \quad (\text{A } -70)$$

Substituting (A – 61) and (A – 70) into (A – 71) gives an expression for the specific thermomechanical (physical) exergy as

$$e_{tm} = C_p(T - T_0) - T_0 C_p \left[\ln \left(\frac{T}{T_0} \right) - \left(\frac{k-1}{k} \right) \ln \left(\frac{P}{P_0} \right) \right] \quad (\text{A } -71)$$

Simplifying (A – 71) further yields

$$e_{tm} = C_p T_0 \left[\frac{T}{T_0} - 1 - \ln \left(\frac{T}{T_0} \right) + \ln \left(\frac{P}{P_0} \right)^{\left(\frac{k-1}{k} \right)} \right] \quad (\text{A } -72)$$

By substituting (A – 72) into (A – 60) we obtain the total specific exergy:

$$e = \frac{1}{2} v^2 + gZ + C_p T_0 \left[\frac{T}{T_0} - 1 - \ln \left(\frac{T}{T_0} \right) + \ln \left(\frac{P}{P_0} \right)^{\left(\frac{k-1}{k} \right)} \right] + RT_0 \ln \left(\frac{P_0}{P_{00,i}} \right) \quad (\text{A } -73)$$

Hence, substituting (A – 73) into (A – 55) gives the overall total exergy rate equation that can be used for calculating the exergy of each component in the model equation:

$$\hat{E} = \frac{1}{2} m v^2 + mgZ + m C_p T_0 \left[\frac{T}{T_0} - 1 - \ln \left(\frac{T}{T_0} \right) + \ln \left(\frac{P}{P_0} \right)^{\left(\frac{k-1}{k} \right)} \right] + m R T_0 \ln \left(\frac{P_0}{P_{00,i}} \right) \quad (\text{A } -74)$$

From a thermodynamics point of view, the exergetic efficiency, which is known as second law efficiency, gives the true value of the performance of an energy system. Exergy is defined as the maximum amount of work obtainable from a system or a flow of matter when it is brought to equilibrium with the reference environment. The exergy consumption during a process is proportional to the entropy production due to irreversibilities. It is a useful tool for furthering the goal of more efficient energy use, as it enables the determination of the location, type, and true magnitude of energy wastes and losses in a system.

For a PEM fuel cell system, the exergetic efficiency is defined as:

$$\varepsilon = \frac{\text{electrical output}}{(\text{exergy})_{Rxtnt} - (\text{exergy})_{Prdct}} \quad (\text{A } -75)$$

$$\varepsilon = \frac{\hat{W}_{net}}{(\hat{E}_{O_2,R} + \hat{E}_{H_2,R}) - (\hat{E}_{O_2,P} + \hat{E}_{H_2O,P})} \quad (\text{A } -76)$$

Appendix A

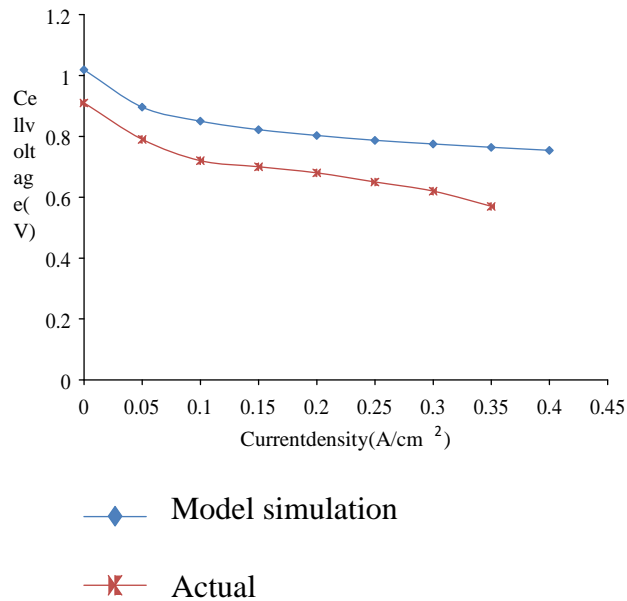


Figure 3: Comparative polarization curve of the simulated and literature results for PEMFC.

where $\hat{E}_{O_2,R}$, $\hat{E}_{H_2,R}$, $\hat{E}_{O_2,P}$ and $\hat{E}_{H_2O,P}$ are the total exergies of the reactants, oxygen, and fuel (hydrogen), and the products oxygen and water, respectively. The net electrical power output produced by the cell is given as

$$\hat{W}_{net} = V_{Cell} * I \quad (A-77)$$

where V_{Cell} is the fuel cell output voltage and I is the current. The computer simulation of the model developed for theoretical energy and exergy analyses of the proton exchange membrane fuel cell is achieved using computer codes to demonstrate the performance and behaviour of the system by varying the operating parameters.

Appendix B DC air conditioner technical specifications:

Table 1 split-type DC Variable frequency Air Conditioner SP4D technical specifications [27]

Item	Specifications
Rated voltage	-48 V DC (-44 V DC to -57 V DC)
Rated refrigeration capacity (L35°C/L35°C)	4000 W
Rated refrigeration capacity (L35°C/L55°C)	2800W
Rated power(L35°C/L35°C)	960 W/20A
Rated power (35°C/L55°C)	1100 W/23A
Maximum current	28A
Refrigerant	R134a/1200g
Energy efficiency ratio(EER,L35°C/L35°C)	4.1
Energy efficiency ratio(EER,L35°C,L°55C)	2.5
Control mode	Smart control
Temperature setting range (controlled by the ECC500)	20-50°C
Temperature setting range (manually)	20-40°C
Environment condition	T3
Ambient temperature range	-15°C to +55°C
Humidity	5%-95% RH
Storage environment	-20°C to +70°C,0-95%RH
Maximum noise	61(dB/A)
Indoor unit noise	59(dB/A)
Outdoor unit noise	61(dB/A)
Outdoor unit protection level	IPX4
Service life	Eight year
Indoor unit dimension (H x W x D)	320 mm x 1045 mm x 210m
Outdoor unit temperature (H x W x D)	528 mm x 766 mm x 278 mm

Bibliography:

- [1]. Rob Harwood, Director Industry Marketing, ANSYS. A New Electrification Revolution.
- [2]. Energy Access Outlook 2017.
- [3]. <http://energyaccess.org/news/recent-news/microgrids-mini-grids-and-nanogrids-an-emerging-energy-access-solution-ecosystem/>.
- [4]. IRENA (2019). Renewable capacity statistics . Abu Dhabi : International Renewable Energy Agency (IRENA), 2019.
- [5]. Zirin, Harold. Solar radiation. ENCYCLOPEDIA BRITANNICA.
- [6]. Types of Solar Cells and Application. Askari Mohammad Bagher, Mirzaei Mahmoud Abadi Vahid, Mirhabibi Mohsen. s.l. : American Journal of Optics and Photonics, Vol. 3, No. 5, 2015, pp. 94-113.doi: 10.11648/j.ajop.20150305.17.
- [7]. <http://windeis.anl.gov/guide/basics/>.
- [8]. World Energy Council 2016. World Energy Resources 2016. 62–64 Cornhill London EC3V 3NH : World Energy Council, Company Limited by Guarantee , 2016.
- [9]. Lawson, Barrie. Battery and Energy Technologies. Electropaedia. [Online] www.mpoweruk.com.
- [10]. Farouk Chellali, Adballah Khellaf, Adel Belouchrani, Abdelmadjid Recioui. A contribution in the actualization of wind map of Algeria. Renewable and Sustainable Energy Reviews. Elsevier, February 2011.
- [11]. <https://www.ecomena.org/renewables-algeria/>.

[12]. google. goole earth. 2019.

[13]. HOMER® Energy. User Manual . HOMER® Pro Version 3.7 . 1790 30th St Suite 100 Boulder CO 80301 USA : s.n., August 2016 .

[14]. Mukund R Patel. Wind and Solar Power Systems: Design, Analysis, and Operation, CRC, 2005.

[15]. Roger A Messenger & Jerry Ventre. Photovoltaic Systems Engineering. CRC, 2003.

[16]. Dolf Gielen. Electricity Storage and Renewables for Island Power, a Guide for Decision Makers. IRENA, 2012.

[17]. JL Gray, A Luque, and S Hegedus. Handbook of Photovoltaic Science and Engineering. Eds. West Sussex, England: John Wiley & Sons, 2003.

[14]. Farshid Mostofi and Hossein Shayeghi. Feasibility and Optimal Reliable Design of Renewable Hybrid Energy System for Rural Electrification in Iran, International Journal of Renewable Energy Research, 2(4), 574–582, 2012.

[19]. Solmetric corporation. Guide to Interpreting I-V Curve Measurements of PV Arrays, Solmetric, 2011.

[20]. A Kaabeche, M Belhamel, and R Ibtouen. Optimal Sizing Method for Standalone Hybrid PV/Wind Power Generation System. Revue des Energies Renouvelables (SMEE'10) Bou Ismail Tipaza, pages 205– 213, 2010.

[21]. Said Diaf, Djamila Diaf, Mayouf Belhamel, Mourad Haddadi, and Alain Louche. A Methodology for Optimal sSizing of Autonomous Hybrid PV/Wind System. Energy Policy, 35(11):5708–5718, 2007.

- [22]. William Brooks & James Dunlop. Photovoltaic Installation Resource Guide, NABCEP, 2012. .
- [23]. Recayi Pecen, MD Salim, and Marc Timmerman. A Hybrid Solar-Wind Power Generation System as an Instructional Resource for Industrial Technology Students. *Journal of Industrial technology*, 16(3):1–7, 2000.
- [24]. Caisheng Wang. Modeling and Control of Hybrid Wind/Photovoltaic/Fuel cell Distributed Generation Systems, PhD thesis, Montana State University, Bozeman, 2006.
- [25]. Pramod Jain. Wind Energy Engineering. McGraw-Hill, 2011.
- [26]. Hermann-Josef Wagner, Jyotirmay Mathur. Introduction to Wind Energy Systems: Basics, Technology and Operation, Springer and 2009.
- [27]. Theoretical energy and exergy analysis of proton exchange membrane fuel cell by computer simulation. D.gimba, A.S.abdulkarimee.A.jimoh,and A.S.Afolbi. s.l. : *Journal of applied chemistry*, 2016, Vol. 2016. 2684919,15pages.
- [28]. User manual Huawei Proprietary and Confidential Copyright © Huawei Technologies Co., Ltd.Issue 05 (2016-06-16) ,page 8

ملخص:

أصبحت الأنظمة الهجينة المعزولة عن الشبكة الكهربائية الحل الأمثل لتزويد المناطق المعزولة وخاصة القرى البعيدة بالكهرباء وذلك لعدت أسباب من بينها موثوقية جودتها، ثباتها وحفاظها على البيئة.

تهدف هذه المذكرة إلى تقديم دراسة لإنشاء شبكة كهربائية مصغرة لتزويد ناقل خلوي بالكهرباء تعتمد على مصادر طاقة كلها متجددة وهي : الألواح الكهروضوئية ، توربين الرياح وخلية الوقود

الكلمات المفتاحية : برنامج هومر، أنظمة الطاقة الهجينة ، سرعة الرياح، الإشعاعات الشمسية ، محرك رياح، طاقة كهروضوئية، نظام طاقة معزول، شبكة كهرباء مصغرة، طاقات متجددة.

Abstract :

Off the grid hybrid systems have been attracting to supply electricity to remote areas in all aspects like, reliability, sustainability and environmental protections, especially for communities living far in areas where grid extension is not appropriate.

This thesis is study aimed to design an optimal off-grid system for remote area in the Algerian desert to power a cellular site based on PV, wind turbine and fuel cell system .

Keywords: HOMER, Wind Speed sources, Solar Radiation, Off-grid power System, Wind/Solar PV/fuel cell /FCPEM/diesel generator, primary load ,NPC, COE, standalone system, mini grid, Renewable energy fraction.

Résumé:

Les systèmes hybrides hors réseau incitent à fournir de l'électricité aux zones isolées sous tous leurs aspects, tels que la fiabilité, la durabilité et la protection de l'environnement, en particulier pour les communautés vivant loin des zones où l'extension du réseau n'est pas appropriée.

Ce mémoire est une étude qui visait à dimensionner un système optimal hors réseau pour une zone isolée du désert algérien afin d'alimenter une antenne-relais , basé sur un système PV, une éolienne et un système de pile à combustible.

Mots clé: HOMER, sources de vitesse du vent, rayonnement solaire, système hors réseau, éolien / solaire PV / pile à combustible / FCPEM / générateur diesel, charge primaire, NPC, COE, système autonome, mini-réseau, fraction d'énergie renouvelable.